Technical Innovations in Pelvic Floor Ultrasonography

Magdalena Maria Woźniak, Andrzej P. Wieczorek, Giulio Aniello Santoro, Aleksandra Stankiewicz, Jakob Scholbach, and Michał Chlebiej

Learning Objectives
- To familiarize with recent ultrasound technical innovations including three-dimensional volume render mode, maximum intensity projection, manual segmentation and sculpting, fusion imaging, PixelFlux, framing, color vector mapping, motion tracking, elastography, contrast-enhanced ultrasound, and automatic calculation systems.
- To understand the future potential of ultrasound technical innovations in clinical practice.

9.1 Introduction

Recently, several new ultrasound techniques have been developed that could significantly improve the diagnostic value of ultrasonography (US) in pelvic floor disorders. Three-dimensional (3D) and real-time four-dimensional (4D) imaging have been introduced into routine medical practice [1–4]. These techniques overcome some of the difficulties and limitations associated with conventional two-dimensional (2D) US. Although 2D cross-sectional images may provide valuable information, it is often difficult to interpret the relationship between different pelvic floor structures because the 3D anatomy must be reconstructed mentally. Three-dimensional reconstructions may closely resemble the real 3D anatomy and can therefore significantly improve the assessment of normal and pathologic anatomy. Complex information on the exact location, extent, and relation of relevant pelvic structures can be displayed in a single 3D image. Interactive manipulation of the 3D data on the computer also increases the ability to assess critical details.

In this chapter the new methods of 3D-US, including volume render mode (VRM), maximum intensity projection (MIP), and brush/shaving options with manual segmentation (sculpting), will be described. A variety of other advanced ultrasonographic techniques, including fusion imaging, PixelFlux, framing, color vector mapping, motion tracking, elastography, contrast-enhanced ultrasound, and automatic calculation systems, will also be presented. It seems likely that these new diagnostic tools will be increasingly used in the future to provide more detailed information on the morphology and function of examined organs, to facilitate planning and monitoring of operations, and for surgical training.

9.2 Volume Render Mode

Volume render mode is a technique for analysis of the information inside a 3D volume by digitally enhancing individual voxels [1]. It is currently one of the most advanced and computer-intensive rendering algorithms available for computed tomography (CT) scanning [5, 6] and can also be applied to high-resolution 3D-US data volume [1, 6]. Four fundamental post-processing functions

M. M. Woźniak (✉) · A. P. Wieczorek
Department of Pediatric Radiology, Medical University of Lublin, Children's University Hospital, Lublin, Poland
e-mail: mwozniak@hoga.pl; wieczornyp@interia.pl

G. A. Santoro
Tertiary Referral Pelvic Floor and Incontinence Center, IV°Division of General Surgery, Regional Hospital, Treviso, University of Padua, Padua, Italy
e-mail: giulioasantoro@yahoo.com

A. Stankiewicz
Imaging Department, University Hospitals of North Midlands NHS Trust, Keele University, Stoke-on-Trent, UK
e-mail: Ola.Stankiewicz@uhnm.nhs.uk

J. Scholbach
Mathematisches Institut, Westfälische Wilhelms-Universität Münster, Münster, Germany
e-mail: contact@chameleon-software.de

M. Chlebiej
Faculty of Mathematics and Computer Science, Nicolaus Copernicus University in Toruń, Toruń, Poland
e-mail: meow@mat.umk.pl

can be used in VRM: opacity, luminance, thickness, and filter. By using these different post-processing display parameters, the volume-rendered image provides better visualization when there are not any large differences in the signal levels of pathologic structures compared with surrounding tissues [1]. Thus, it is successfully applied for more precise assessment of some pathological conditions, such as anal sphincter defects, fistulous tracts in perianal sepsis (Fig. 9.1), and invasiveness of the submucosal layer in early rectal cancer [7]. Moreover, it seems to be a very promising method for detailed evaluation of the integrity of or injuries to the pelvic floor muscles (Figs. 9.2, 9.3, and 9.6), visualization of the spatial distribution of the vascular networks supplying the urethra, and assessment of the location of tapes or meshes after pelvic floor surgery (Figs. 9.4 and 9.5). Most recent advanced volume render mode includes volume-rendering mode of four-dimensional translabial ultrasound; this technique appeared very useful in the assessment of the association between a widened vaginal canal with concealed uterine prolapse [8] (Fig. 9.6).
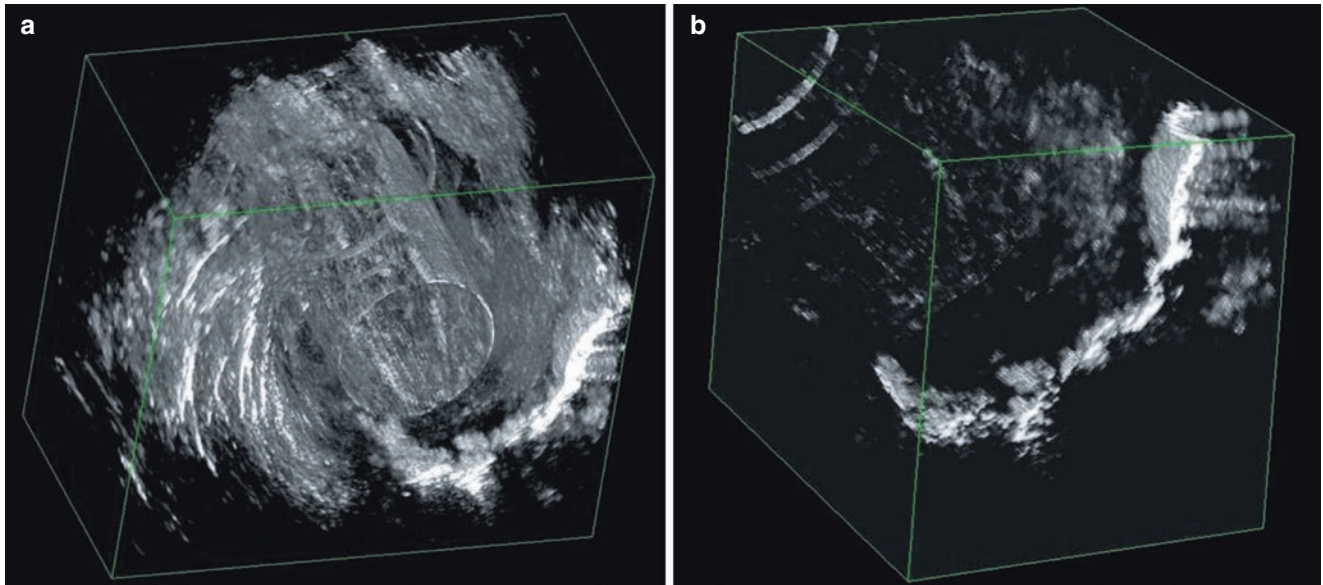

Fig. 9.1 Effects of image processing (volume render mode with filtering) on fistula tract views after hydrogen peroxide injection through an external opening (**a**, **b**). Scan obtained by endoanal ultrasound with 2050 transducer (BK Medical)
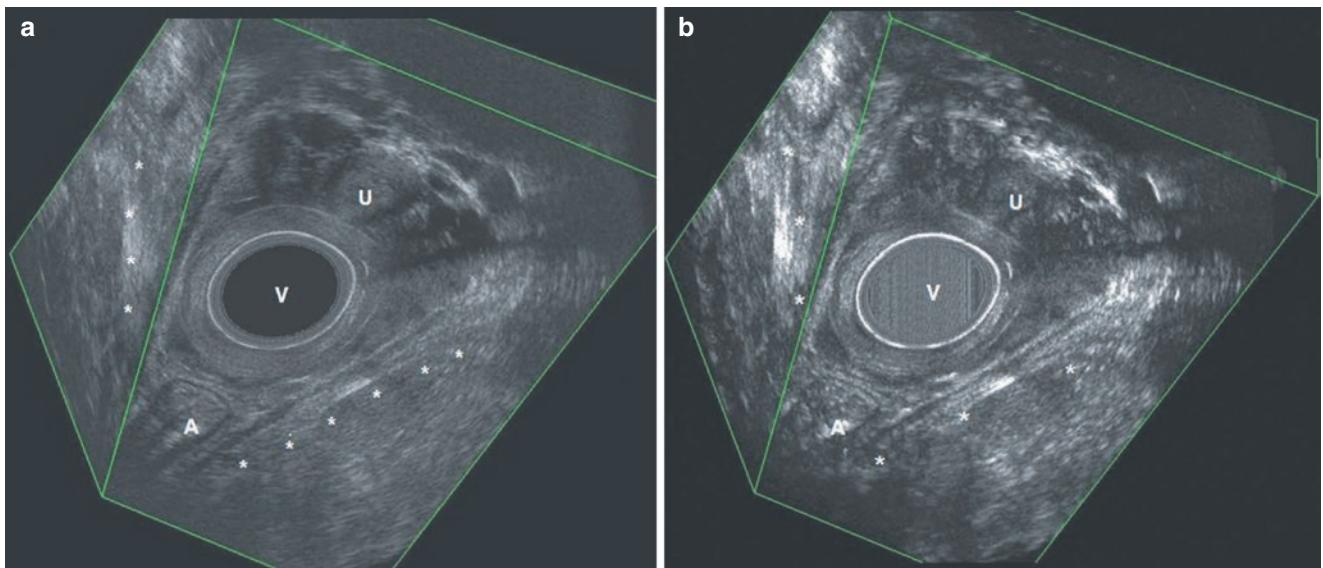

Fig. 9.2 (**a**) Visualization of the puborectalis muscle in different oblique planes (∗). (**b**) Post-processing manipulation (volume render mode with high opacity and luminance) improves the visibility of the muscle. *A* anal canal, *U* urethra, *V* transducer into vagina. Scan obtained by endovaginal ultrasound with 2050 transducer (BK Medical)
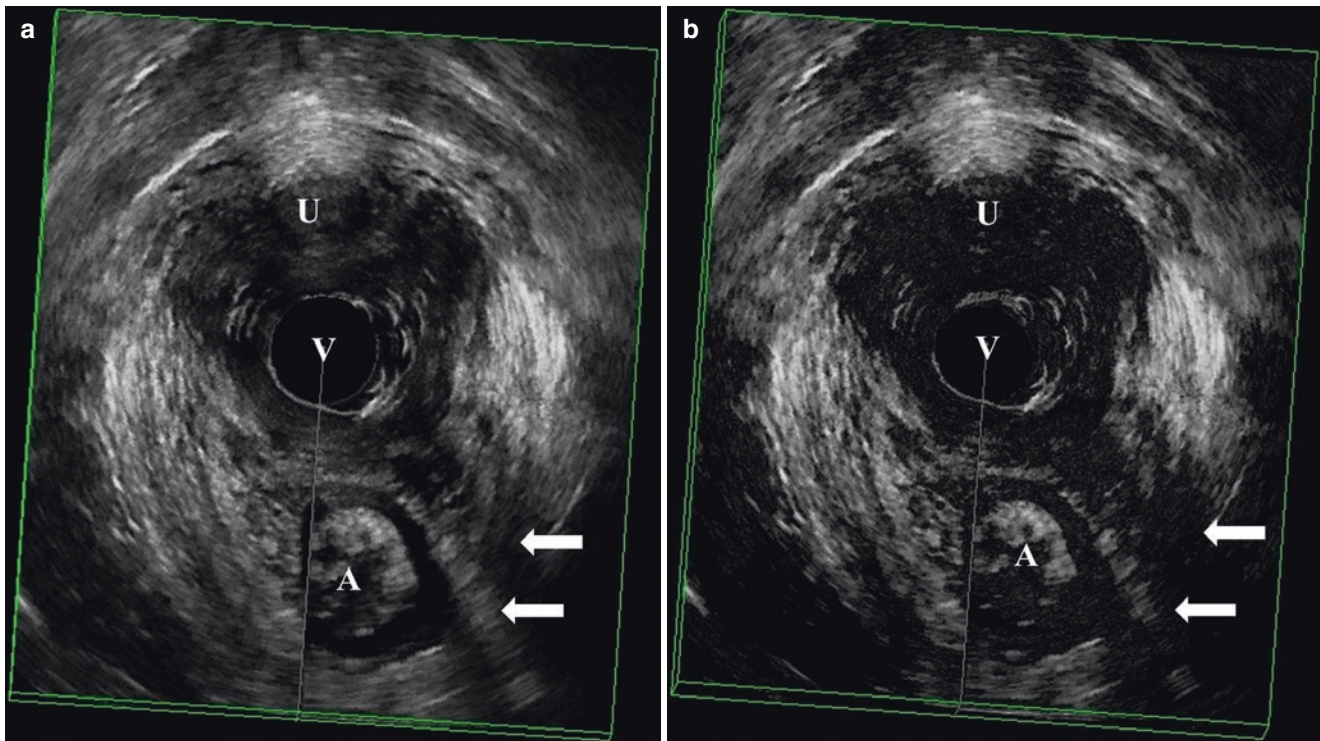
Fig. 9.3 Visualization of puborectalis muscle showing defect on the left side (white arrows). (**a**) Normal mode, (**b**) volume render mode. *A* anal canal, *U* urethra, *V* transducer into vagina. Scan obtained by endovaginal ultrasound with X14L4 transducer (BK Medical)
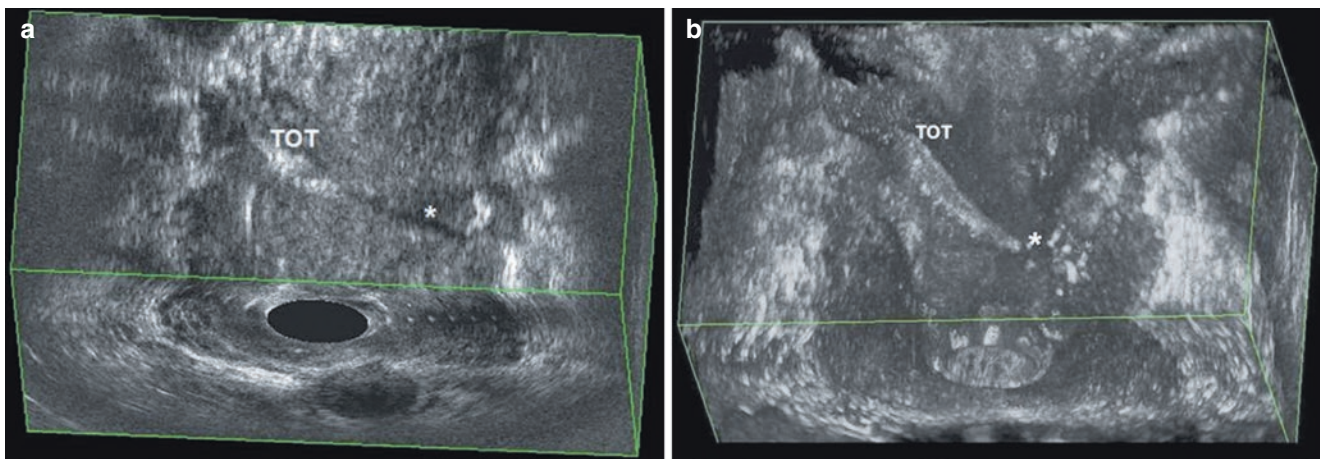

Fig. 9.4 Visualization of the position of a trans-obturator tape (*TOT*) in the coronal plane. In the left side, the sling appears dislodged (∗). (**a**) Normal mode, (**b**) volume render mode. Scan obtained by endovaginal ultrasound with 2050 transducer (BK Medical)

9.3 Maximum Intensity Projection

Maximum intensity projection (MIP) is a 3D visualization modality involving a large amount of computation [3]. It can be defined as the aggregate exposure at each point, which tries to find the brightest or most significant color or intensity along an ultrasound beam. Once the beam is projected through the entire volume, the value displayed on the screen is the maximum intensity value found (the highest value of gray or the highest value associated with a color). Conversely, if the value displayed on the screen is the minimum value found, this is termed minimum intensity projection (MinIP).

It has been reported in the literature that the application of MIP to 3D color US allows visualization of the distribution of blood vessels in tumors, providing additional information for management. Ohishi et al. [9] found that 3D images with MIP
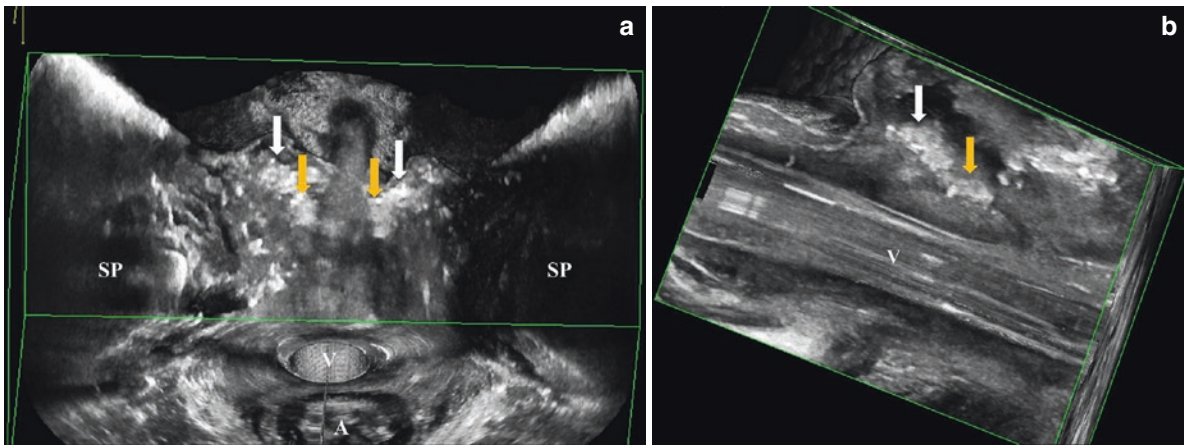
Fig. 9.5 Visualization of the position of two trans-obturator tapes (*TOT*) in volume render mode (marked with white and yellow arrows). (**a**) The coronal plane, (**b**) the sagittal plane. *A* anal canal, *SP* symphysis pubis, *V* transducer into vagina. Scan obtained by endovaginal ultrasound with X14L4 transducer (BK Medical)
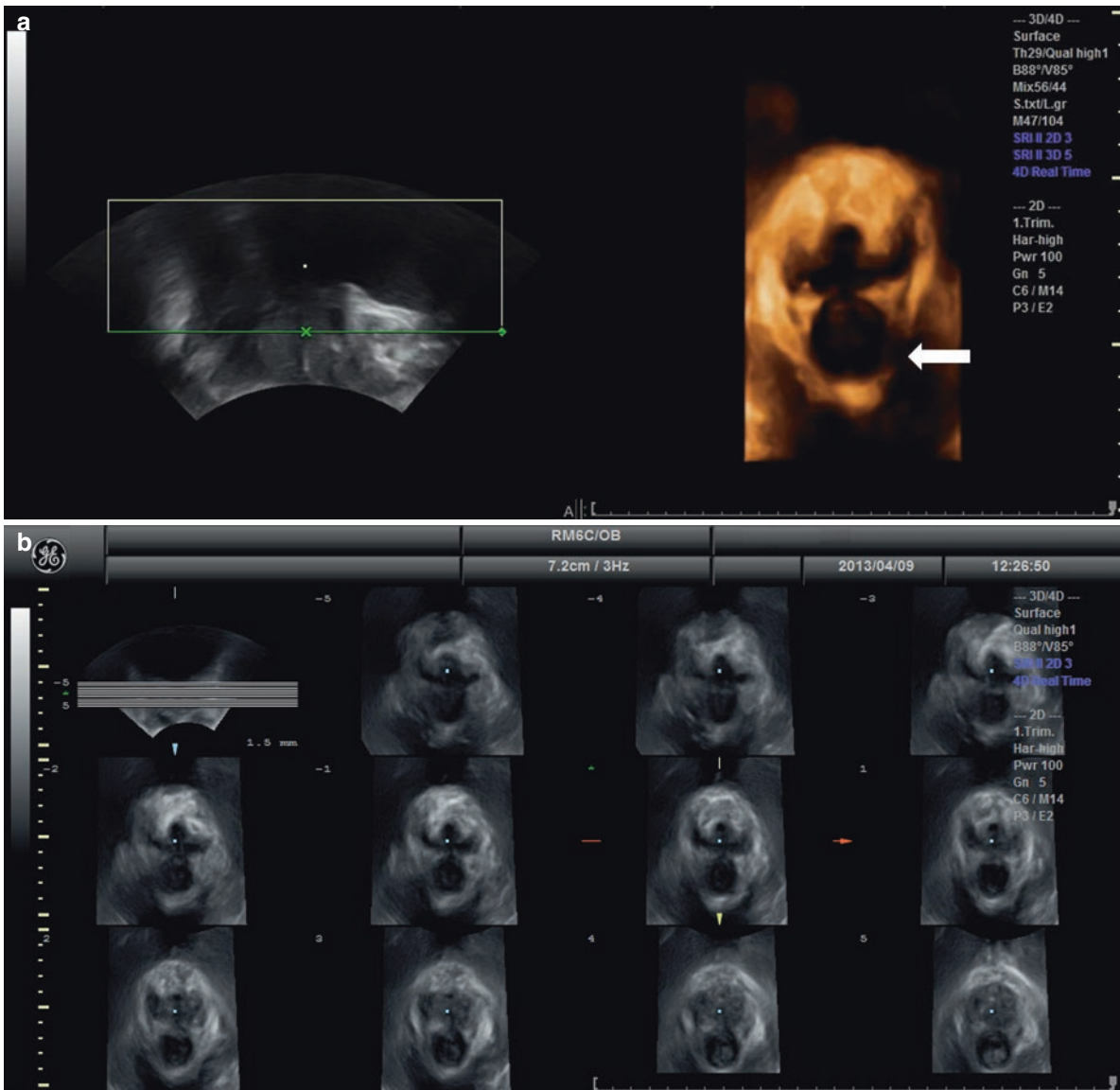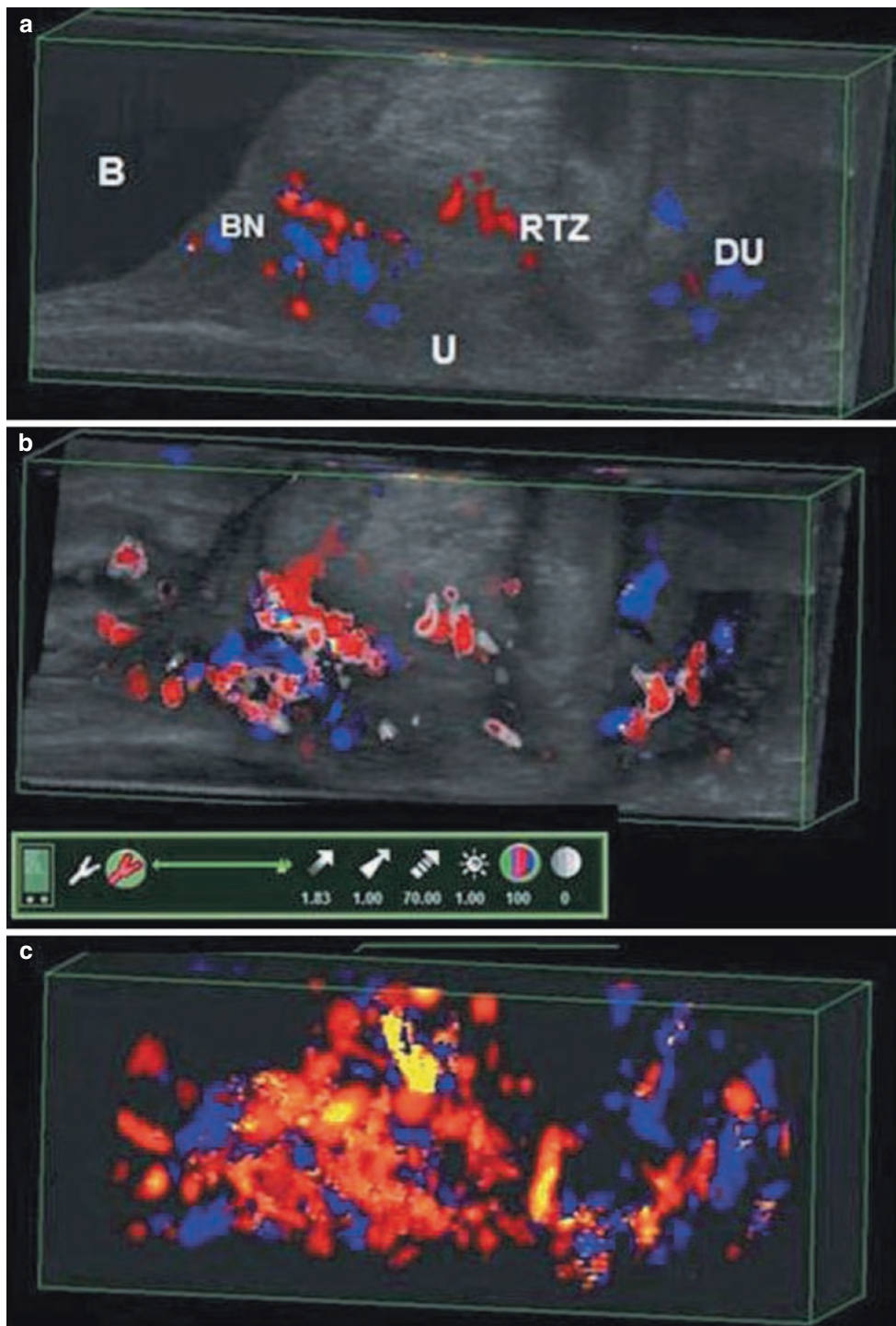

Fig. 9.6 Visualization of hiatus with a 4D transperineal ultrasound (TPUS) showing left-sided defect (white arrows). (**a**) Surface render mode, (**b**) tomographic ultrasound imaging (TUI). Scan obtained by transperineal ultrasound with RM6C transducer (General Electric)

mode improved evaluation of the entire vasculature of a tumor compared to cross-sectional 2D images. Hamazaki et al. [10] reported that 3D color Doppler US with MIP mode appeared to be useful for the differential diagnosis of subpleural lesions. Motohide et al. [11] considered this technique an efficient and safe modality as an intraoperative navigation system for liver surgery. In a preliminary study in nulliparous females, we found that application of MIP reconstruction allowed visualization of the patterns of urethral vessels (spatial distribution and localization of vessels) (Fig. 9.7) [12].

9.4   Brush Options: Segmentation—Sculpting

Sculpting is a post-processing tool that allows the examiner to mark volume voxels, during off-line assessment of 3D-US imaging (version 7.0.0.518—BK Medical 3D Viewer), so that they are not displayed in the rendering operations. The marking process uses a standard projection method to map screen locations within a boundary of the volume data. There are two methods available: (1) in the first technique, the vox-

Fig. 9.7 Midsagittal view of urethral vasculature with color Doppler mode (**a**), normal render mode (**b**), and maximum intensity projection (**c**). *B* bladder, *BN* bladder neck, *DU* distal urethra, *RTZ* Retzius plexus, *U* urethra. Scan obtained by endovaginal ultrasound with 8848 transducer (BK Medical)

els are marked in a mirror volume which gives the possibility of turning the marking on and off or inverting it; (2) in the second technique, the voxels are replaced with some marker value. This method requires reloading of the volume to turn off the sculpting.

Various sculpting tools are possible, giving different degrees of control over what is removed: (1) to draw an outline and then remove everything within that outline to a given depth or through the entire volume; (2) to draw an outline and then remove everything outside the outline; or (3) to use a shaving tool that marks a few voxels at a time around the point of the cursor. The depth of sculpting can be a percentage of the total or a given value in millimeters from the surface of the volume. As pelvic structures vary in shape and lie in different oblique planes, we recommend performing a sculpting on every section of some millimeters' length or even on every image of 300 transaxial images collected during 3D data acquisition (Figs. 9.8 and 9.9). Sculpting was originally developed for enhancing static volumes of the fetus by removing the placenta [13]. Its introduction into pelvic imaging might facilitate the assessment of pelvic floor structures (Figs. 9.10 and 9.11), allowing comparison of the morphology in different disorders.

9.5 Fusion Imaging

Fusion imaging is based on a simultaneous capturing of scans obtained by two different examinations, e.g., CT/MRI (magnetic resonance imaging), US/MRI, CT-PET (positron emission tomography), and MRI-PET, providing the information gathered by both modalities fused. This technique ensures a compensation for the deficiencies of one method and retains the advantages of another one. Fusion imaging is performed by using dedicated software, on a graphic workstation, where the data are transferred using the Digital Imaging and Communications in Medicine (DICOM) system. The volume-rendering mode allows simultaneous projection of the 3D dataset of two different studies to be fused. The datasets are labeled with color to allow the user to identify the separate studies. The color labeling is arbitrary and depends on the user's preference. The registration process requires an individual manipulation and is achieved by superimposing the two datasets with the use of 3D volume projection. It is, however, mostly conducted in the 2D slice views, due to easier visualization of the superimposed datasets, and in the transverse planes, as these provide better scanning resolution. The user works in the standard directions of sagittal, coronal, and transverse and updates the registration in each of these views. Final image registration is based on anatomical adjustment of the imaging studies (Fig. 9.11).

Fusion imaging is commonly used in the diagnosis of cancer patients. Kim et al. [14] showed an additional diag-
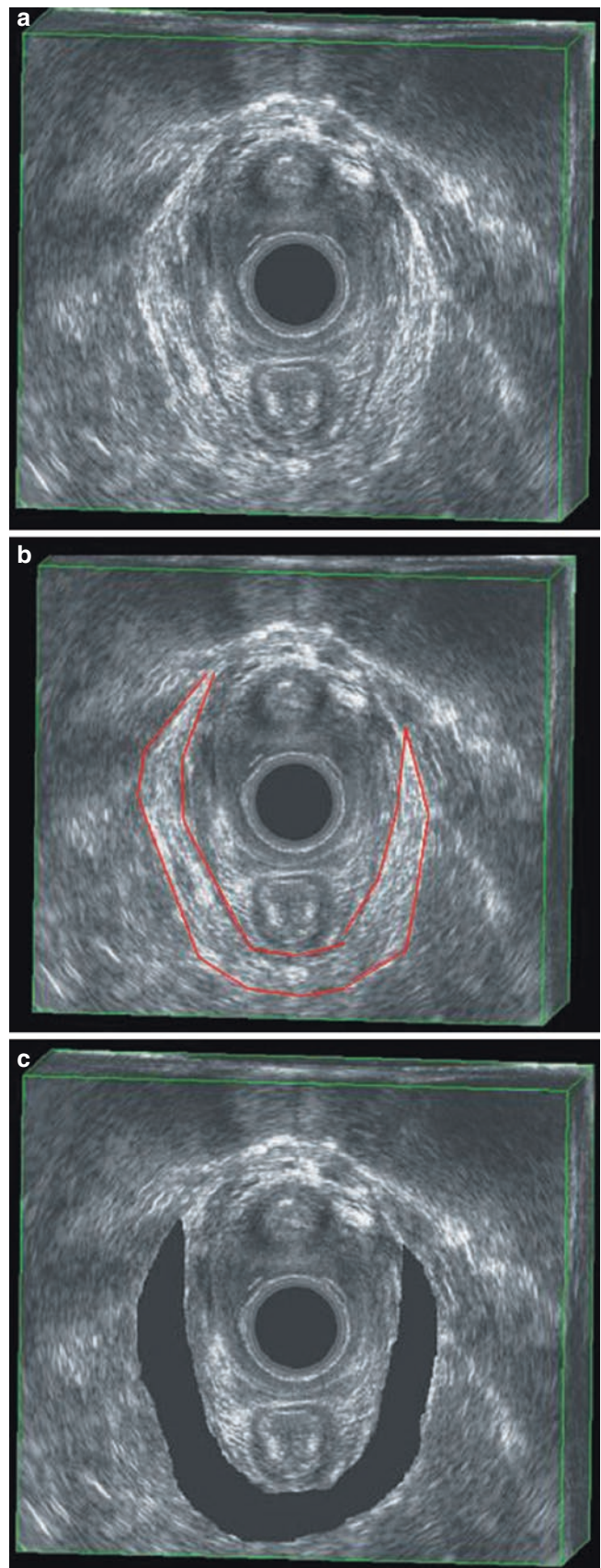

Fig. 9.8 Sculpting of the levator ani muscle. (**a**) Axial view obtained by endovaginal ultrasound with 2050 transducer (BK Medical). (**b**) The outlining of the levator ani muscle. (**c**) The levator ani muscle is removed
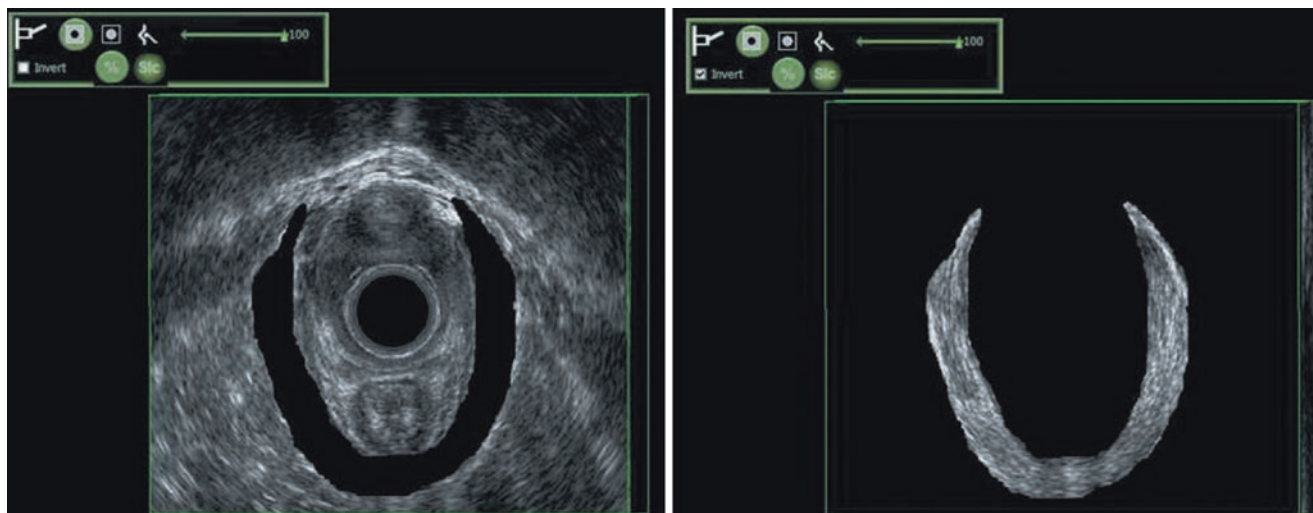
Fig. 9.9 Two methods of sculpting: (1) the levator ani muscle is outlined and is cut off (*left*) and (2) outlining of the levator ani muscle with cutoff of all the structures lying beyond (*right*). Scan obtained by endovaginal ultrasound with 2050 transducer (BK Medical)
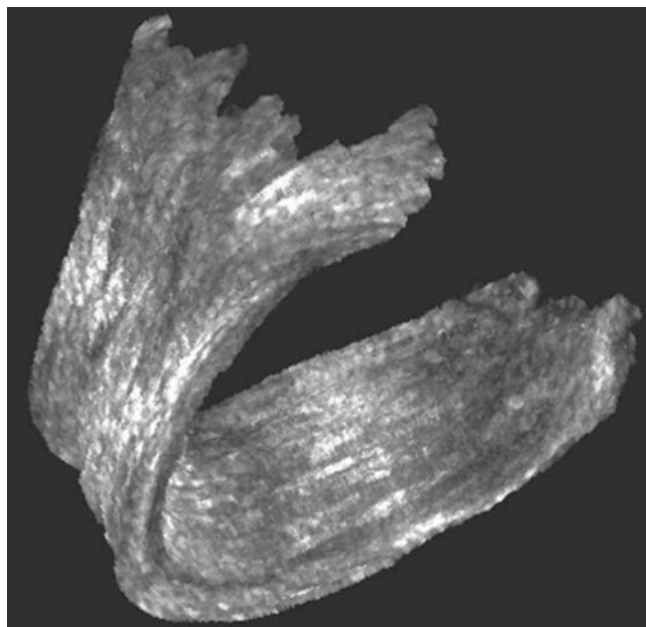

Fig. 9.11 Three-dimensional reconstruction of the middle third of the anal canal using the sculpting method. The two rings of the internal (hypoechoic) and external (hyperechoic) sphincters are clearly visualized. Scan obtained by endoanal ultrasound with 2050 transducer (BK Medical)

Fig. 9.10 Levator ani muscle reconstruction using the sculpting method. Scan obtained by endovaginal ultrasound with 2050 transducer (BK Medical)

nostic value of fused MR/PET images in comparison with PET/CT in the detection of metastatic lymph nodes in patients with uterine cervical cancer. Another study reported that the fusion of real-time transrectal ultrasound (TRUS) and prior MR images of the prostate facilitated MRI-guided interventions such as prostate biopsies, cryoablation, brachytherapy, beam radiation therapy, or direct injection of agents outside of the MRI suite [15]. Moreover, the image fusion between color Doppler TRUS and endorectal MRI appeared to improve the accuracy of pathological staging in patients

with prostate cancer [16]. MRI and TRUS fusion has the potential for follow-up of anorectal fistulae and abscesses and staging of anal and rectal tumors [17].

Similarly, CT/MRI fusion images were performed for abdominal, cervical, and intracranial regions assessment [18].

We assessed the application of US/MRI fusion imaging for the visualization of pelvic floor structures in nulliparous females. For the fusion process, T_1-weighted axial scans were used. Fusion imaging was performed on a laptop with the use of dedicated software, and once it was completed, a 3D reconstruction of the levator ani muscle and the anatomical alignment was conducted (Fig. 9.12). Both methods appeared to be highly concordant in the visualization of this

Fig. 9.12 Axial views of the female pelvis. (**a**) MRI scan. (**b**) Endovaginal ultrasound with 2050 transducer (BK Medical). Both images were captured simultaneously to allow fusion of the info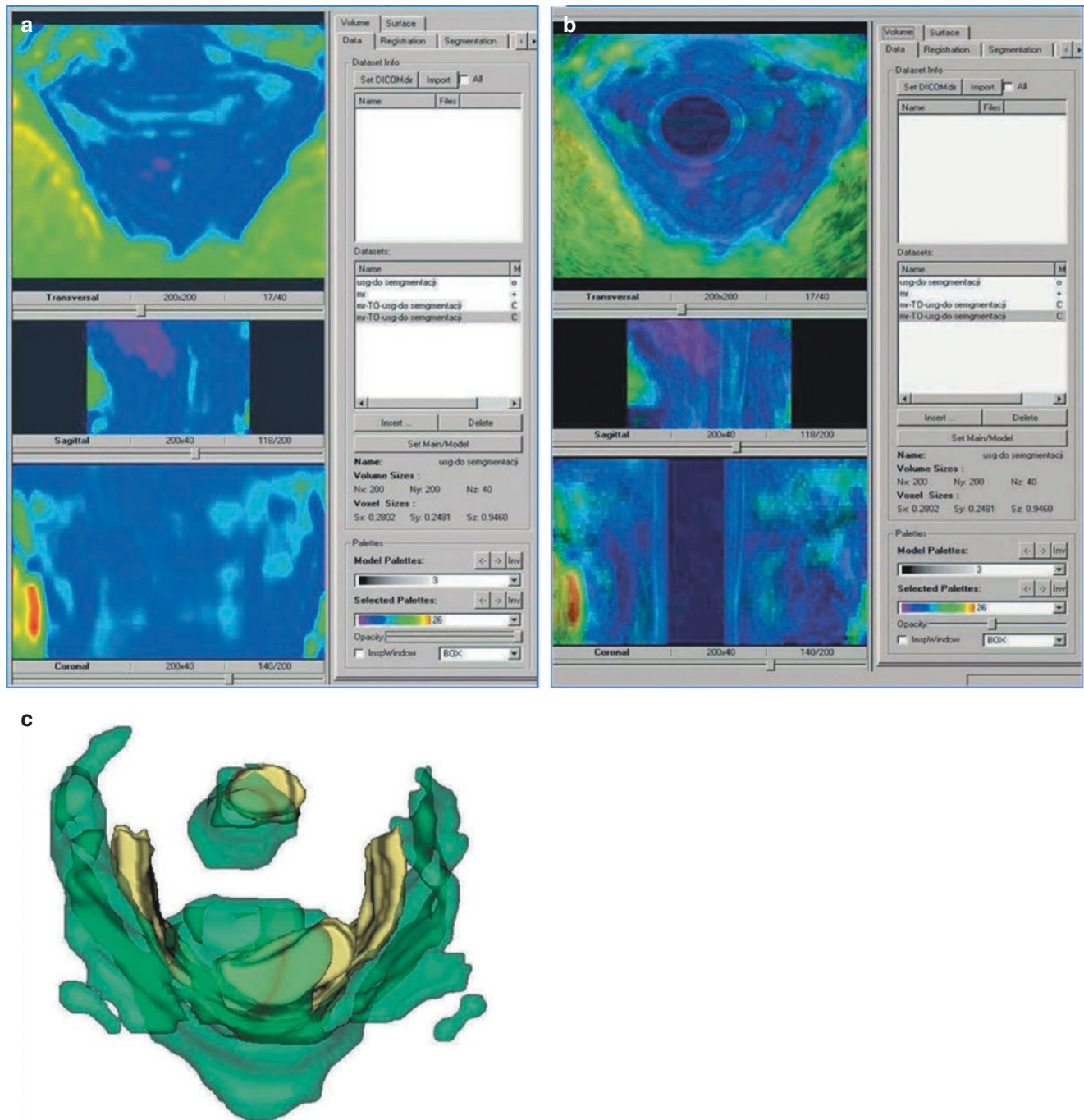rmation provided by each technique. (**c**) Fusion imaging of the three-dimensional reconstruction of the levator ani muscle (*brown*, US image; *green*, MR image)

muscle; however, MRI, due to a wider field of view than the ultrasound transducer, provided more information about surrounding structures.

9.6 PixelFlux

PixelFlux is dedicated software that allows an automated calculation of blood perfusion in arbitrary regions of interest (ROIs) of different organs [19, 20]. The basic principle of this software is the requirement that measurements must be reliable (Fig. 9.13). For this reason:

1. Perfusion measurements should not be influenced by the external settings of the US device. Any parameters that impact the perfusion depiction must be kept constant throughout. One of these parameters is pulse repetition frequency (PRF), higher PRF permits higher Doppler shifts to be detected, and lower PRF allows recording of lower velocities. The calibration of the image, which consists of setting the scale and the maximum Doppler velocity, is automatically provided by the software, particularly when DICOM files are used.
2. Perfusion measurements must not rely on the subjective visual impression of the examiner, as this may lead to serious misinterpretation. To avoid operator dependency,

when opening a video or DICOM file, the software automatically finds the scale indicating the colors used for perfusion depiction and allows a standardized measurement.

Perfusion measurements must yield constant results when comparing the perfusion of the same patient at different times. In order to assess the perfusion in an authentic way, it is thus crucial either to take into account the perfusion in similar points of the cardiac cycle, e.g., by always comparing the systolic or diastolic perfusion, or to compute the "average perfusion" during a complete heart cycle. The key step of the perfusion measurement technique is the definition of the ROI. The ROI can be arbitrarily chosen by the examiner, taking any desired size or shape. ROI can also be defined as a parallelogram, which has proved useful in measuring renal parenchymal perfusion [20], or can be derived from another freehand outlined ROI by a dartboard-like scheme, which is adapted to ring-like structures such as the rhabdosphincter muscle or the inner ring of the urethra, including the longitudinal smooth muscle, the circular smooth muscle, and the submucosa layer of the urethra.

After choosing the ROI, the software automatically calculates the perfusion of the region in every frame of the video assessed. The following parameters are computed: (1) the velocity V, which corresponds to the color hue of the pixels inside the ROI; (2) the perfused area A, given by the amount
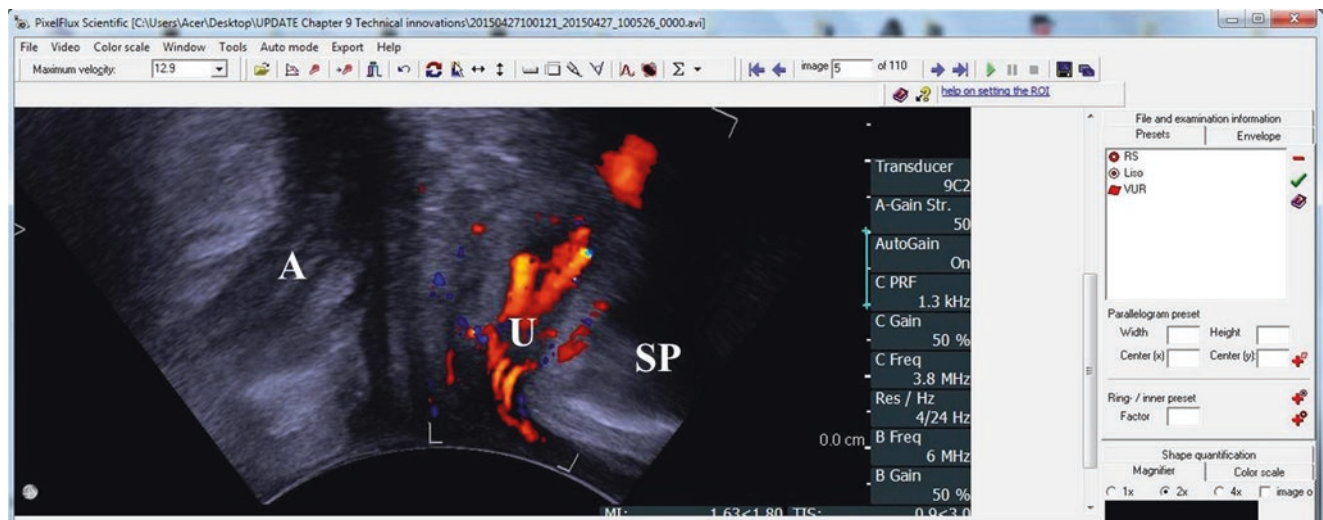

Fig. 9.13 Color Doppler ultrasound for the assessment of the vascularity of the whole urethral complex in PixelFlux. *A* anal canal, *SP* symphysis pubis, *U* urethra. Sagittal scan of the mid-urethra obtained by endovaginal ultrasound with X14L4 transducer (BK Medical)

of perfused pixels inside the ROI; and (3) the perfusion intensity, *I*. This parameter is defined as the ratio:

$$I = V \times A / A_{ROI}$$

where A_{ROI} denotes the total area of the ROI. Consequently, the perfusion intensity increases with the perfusion velocity but decreases if less of the total area of the ROI is globally perfused. These three parameters are computed for each single frame of the video examined. Based on the periodic changes due to the cardiac cycle, the program then automatically calculates the heart period and takes into account only one or multiple full heart cycles. The quantification of complete heart cycles accomplishes the need for a time-independent perfusion measurement as outlined above. Figure 9.14 shows a heart cycle recognized by the software (the parts of the chart highlighted in red and blue, respectively).

Another key parameter of the PixelFlux software is "perfusion relief." It shows the local distribution of perfusion intensity, like a map depicting the height of mountains (Fig. 9.14). This tool can be used to gain a visual impression of the vasculature, showing areas with different local perfusion (Fig. 9.15).

The PixelFlux technique enables a quantitative assessment of blood perfusion. The program is completed by an internal database, facilitating the handling of large amounts of patient data, including features for comparison of different patients or examination of the same patient at different times. It appears a very promising method for evaluating the vasculature of pelvic structures in females at risk for developing urinary incontinence or organ prolapse. In addition, it could be used to analyze the perfusion intensity in women suffering from any pelvic floor disorder, in order to define whether the severity of their symptoms correlates with perfusion parameters.

Using the PixelFlux software for assessment of the blood perfusion in the urethra of nulliparous females, we found that the intramural and distal part of the urethra had poorer vascular intensity than the mid-urethra. Interestingly, we did not observe any difference between the perfusion intensity in the inner (including the longitudinal smooth muscle, the circular smooth muscle, and the submucosa) and outer (corresponding to the rhabdosphincter muscle) rings of the mid-urethra [12, 21]. Lone et al. studied vascularity of the urethra in continent women using color Doppler high-frequency endovaginal ultrasonography and showed that compared to continent nulliparous women, continent multiparous women demonstrated a significant reduction in the vascularity parameters in all measured variables when parity was accounted for [22].
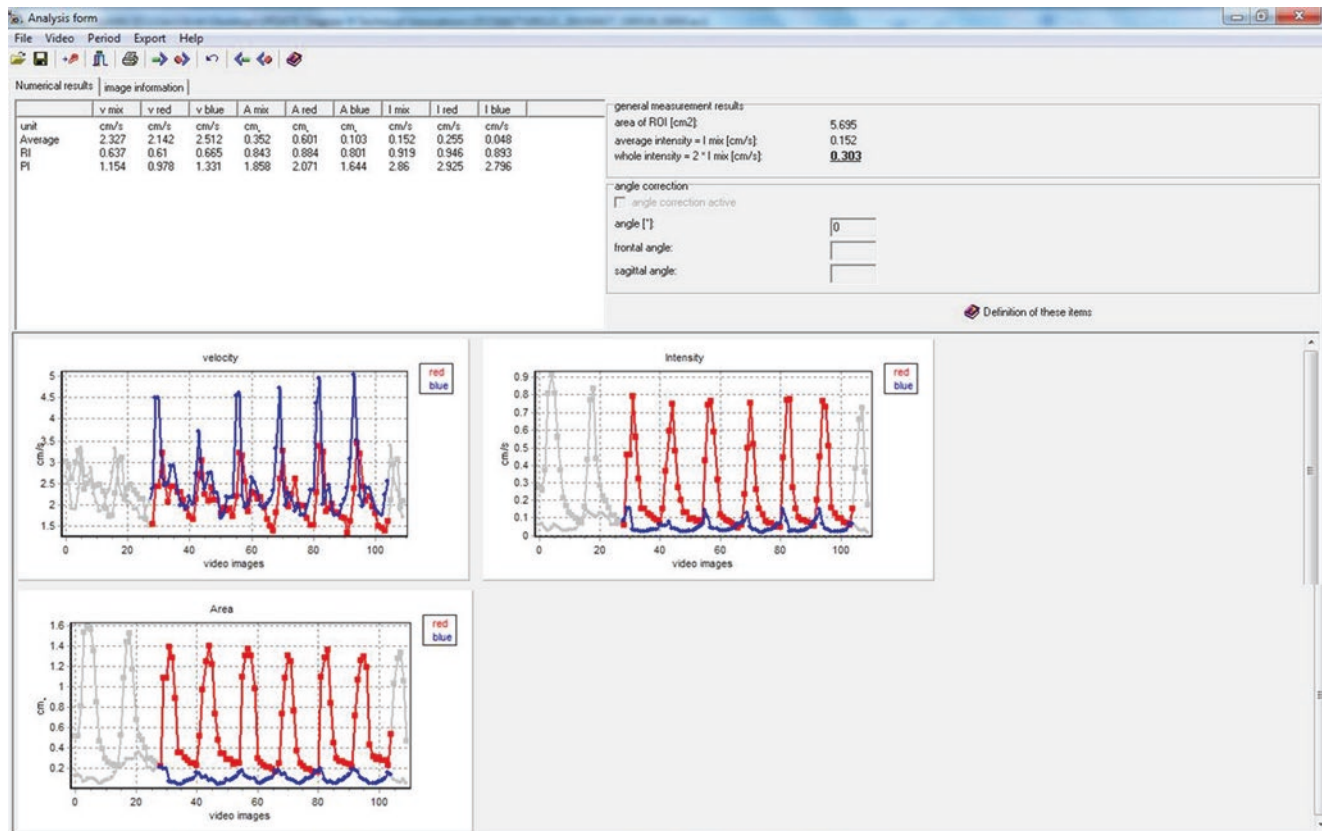

Fig. 9.14 PixelFlux technique. Analysis form shows the heart cycles and the values of velocity, intensity, and area within the region of interest
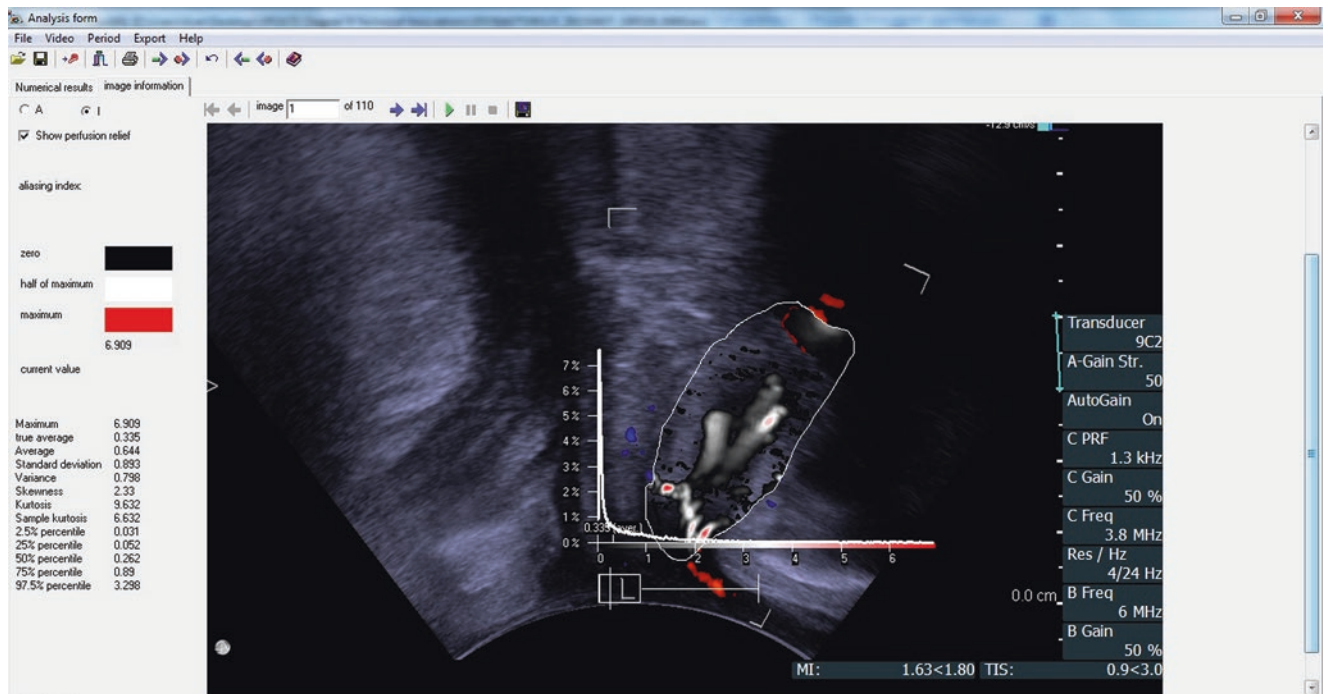
Fig. 9.15 PixelFlux technique. Region of interest includes the mid-urethra. Analysis form showing the local perfusion relief (*red* areas correspond to regions with high perfusion velocity; *white* and *black* areas correspond to regions with moderate or low perfusion velocity). Scan obtained by endovaginal ultrasound with 9C3 transducer (BK Medical)

The same authors in the 1-year prospective follow-up study assessing urethral vascularity using 2D color Doppler high-frequency endovaginal ultrasonography in women treated for symptomatic stress urinary incontinence found out that there is no change in vascularity parameters in women who opt for conservative or surgical treatment of SUI [23]. In the study by Yeniel et al., the authors attempted to find out if overactive bladder microvasculature disease is a component of systemic atherosclerosis and found that all atherosclerosis indicators were significantly associated with OAB and that there was a significant relationship between OAB and decreased bladder neck perfusion. Additionally, there were correlations of OAB severity with systemic atherosclerosis and impaired vascular perfusion of the bladder. Decreased perfusion at the bladder neck, the Framingham scores in severe OAB, and the correlation between them suggest that OAB microvascular disease may be a component of systemic atherosclerosis rather than a separate process [24].

9.7 Framing

The motion of pelvic structures can be observed in real time by using dynamic ultrasound while asking patients in a supine or standing position to strain or to cough. The data can be registered as video files for off-line examination. Dynamic US, however, provides an abundance of information that cannot be captured by the observer alone, as it occurs too fast.

Framing is a modality that provides a detailed visualization of the motion sequences of specific structures. With use of dedicated software (VIRTUAL-DUB), it is possible to analyze consecutive frames of a video file, by cutting off the frame without decompression. It has potential application in the assessment of functional disorders of the pelvic floor.

9.8 Motion Tracking and Color Vector Mapping

Our ability to understand pelvic floor dysfunction arises from understanding the complex functional interactions among pelvic organs, muscles, ligaments, and connective tissue. Dynamic US imaging provides a quantitative evaluation of pelvic floor structures. Measurements of bladder neck displacement, urethral inclination, and retrovesical angle at rest and during pushing or straining give important information in patients with urinary incontinence [25]. However, due to small dimensions and different velocities and movements of the pelvic structures, it is not possible to describe their interactions precisely.

Motion tracking is a modality for the assessment of biomechanical properties of tissues and organs [26]. Computer-aided vector-based perineal ultrasound appears to be a feasible and valuable tool for the assessment of bladder neck mobility, allowing the user to distinguish between women with and without stress urinary incontinence [27, 28]. Peng et al. [29] reported that motion tracking may be used for the assessment of puborectalis and pubococcygeus contraction, by evaluating the displacement of the anorectal angle (ARA) during perineal US. To map accurately the trajectory of the ARA, every frame was indexed to the same rigid landmark (the symphysis pubis—SP). A template of the SP was initially defined in the first frame of the ultrasonographic video file, then it was compared with the second image with different offset in both the x and y direction. The matching procedure employed some equations and was repeated until the last image frame. The relative displacement of the ARA to the SP was obtained by subtraction of the SP from the ARA. Results of this study showed that during cough, the ARA moves toward the SP (ventrally) in continent women and away from the SP (dorsally) in urinary-incontinent patients. In addition, the amplitude of ARA maximal caudal displacement was smaller in continent women compared to incontinent patients [29]. Constantinou [30] described the dynamics of female pelvic floor function using urodynamics, ultrasound imaging with motion tracking, and MR, in terms of determining the mechanism of urinary continence. Among these modalities, motion tracking provided quantitative measures (displacement, velocity, acceleration, trajectory, motility, strain) of pelvic floor muscles. On the basis of these parameters, the status of continent and asymptomatic women could be clearly distinguished from those with incontinence.

We developed a novel computer software for quantitative assessment of the motion of pelvic structures. This software was originally applied to 3D echocardiographic scans to evaluate the kinetics of the cardiac walls in patients with heart infarction [31, 32]. The process of analysis consisted of several main steps:

- Filtering: to improve the US image quality and to remove the noise; the diffusion algorithm was applied, as it dramatically enhances the structure boundaries and reduces the speckle noise.
- Description of the motion: recovery of transformation, which aligns the reference frame with all the other frames using intensity-based 3D volume registration; this allows to visualize local deformation of spatial objects.
- De-noising procedure using time-averaging technique: the deformation fields are used to generate new datasets elastically aligned with the reference frame T0; the noise

in the datasets is smoothed, and the boundaries of the image structures are preserved.
- Segmentation step using the averaged dataset by iterative deformable boundary approach.
- Reconstruction of the motion by applying the deformation field operator.

For description of the motion, vector displacement was calculated as a total displacement (relative to the reference frame T0) and displacement between consequent time frames which can be seen as an instantaneous velocity. To visualize the motion occurring on the surface (twisting), the instantaneous velocity vectors were decomposed into tangential and normal components.

Different techniques can be used to visualize the local variations of the motion as follows:

- Color-based visualization according to length values of displacement vectors. It is the preferred modality when we deal with small moving surfaces.
- Vector-based visualization: for significant motion it is preferred to visualize vector values using the arrows representing the length and spatial orientation of moving matter.
- Line-paths-based visualization: in this method, the small set of surface points is selected, and the path of their motion is visualized. Colors of the line segments represent various time frames. This method enables estimation of the viability of the heart using a single image. In addition to the line-paths method, we may also generate the "activity surface." Using this technique, total path length values (in a single cardiac cycle) for every surface point can be visualized. Thus it allows easy detection of moving regions and evaluation of how significant this motion is, as well as estimation of the spatial extent of pathological regions on single static image. Line-paths visualization contains complete information about the motion, whereas activity surfaces show the overall surface activity more clearly [32].

The motion tracking procedure described above can be applied to assessment of the function of pelvic structures. The data are collected using transperineal and endovaginal ultrasound scanning in B mode, during straining and Valsalva maneuver, and registered as video files. The data are then analyzed with the use of color and vector mapping (Fig. 9.16). We believe that this modality could enhance our knowledge of pelvic organ dysfunction, facilitating the diagnosis of injuries or deficiency of pelvic muscles after childbirth that is not detectable by conventional imaging techniques. It can also be useful to evaluate muscle strength after biofeedback treatment.
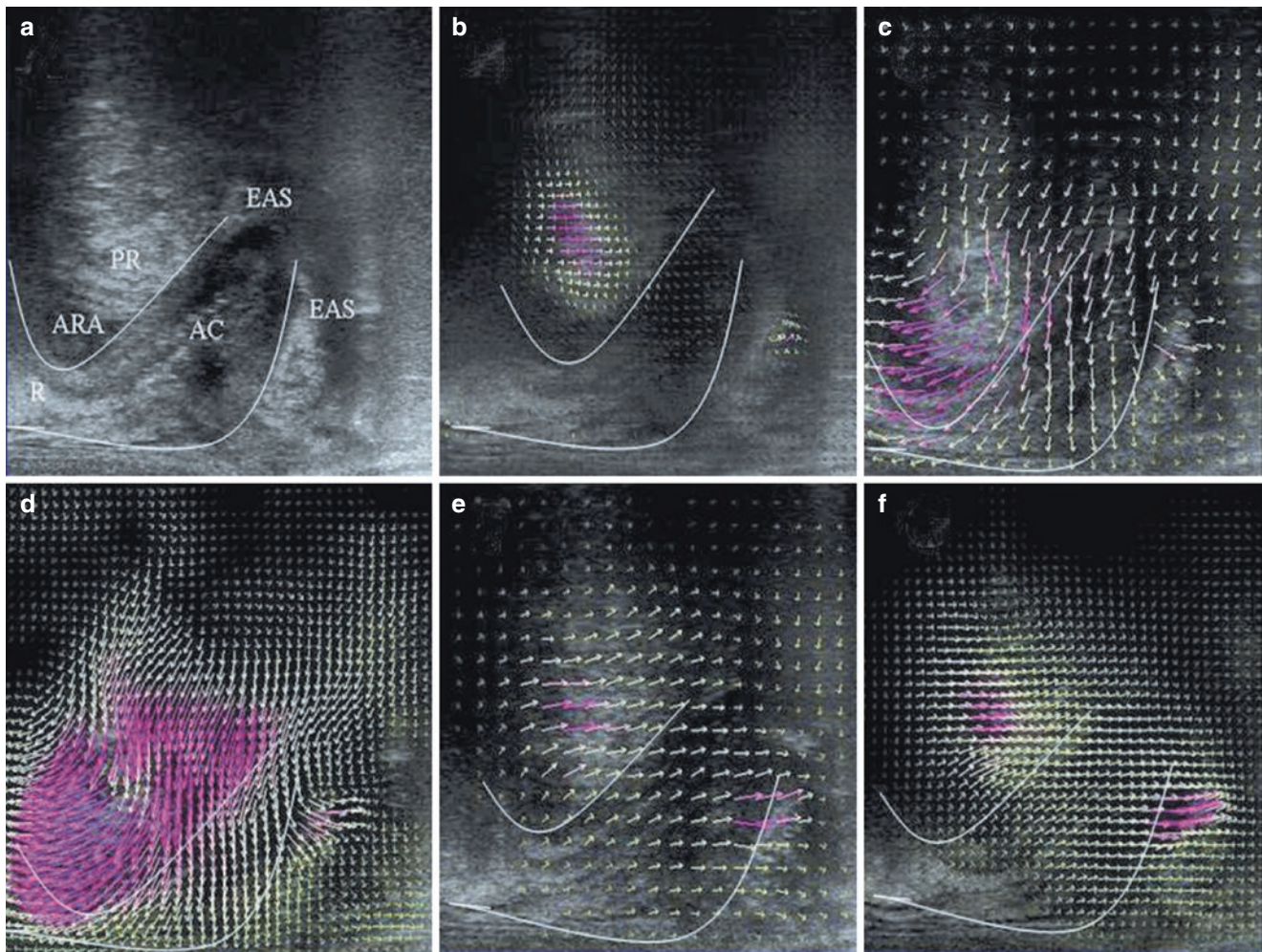
Fig. 9.16 (**a**) Longitudinal section of the posterior compartment. Color and vector mapping were applied for the assessment of the muscles' motion. *AC* anal canal, *ARA* anorectal angle, *EAS* external anal sphincter, *PR* puborectalis muscle, *R* rectum. (**b–d**) During straining, upward movement of the puborectalis is visualized. This movement closes the anorectal angle, assuring continence. (**e**, **f**) During Valsalva maneuver, the puborectalis activity is suppressed, whereas the external sphincter opens. Scans obtained by endovaginal ultrasound with 8848 transducer

9.9 Elastography

Elastography uses ultrasonic imaging to observe tissue shear deformation after applying a force that is either dynamic (e.g., by thumping or vibrating) or varying so slowly that it is considered "quasi-static" (e.g., by probe palpation). The deformation may be represented in an elasticity image (elastogram), or as a local measurement, in one of three ways:

1. tissue displacement which may be detected and displayed directly, as in the method known as acoustic radiation force impulse (ARFI) imaging,
2. tissue strain which may be calculated and displayed, producing what is termed strain elastography (SE), or,

3. in the dynamic case only, the data may be used to record the propagation of shear-waves, which are used to calculate either.

   (a) regional values of their speed (without making images) using methods referred to herein as transient elastography (TE) and point shear-wave elastography (pSWE), or,
   (b) images of their speed using methods referred to herein as shear-wave elastography (SWE) which includes 2D SWE and 3D SWE [33].

The strain measurements (including SE and ARFI) are displayed as a semitransparent color map called an elastogram, which is overlaid on the B-mode image. Typically, low strain (stiff tissue) is displayed in blue, and high strain (soft

tissue) is displayed in red, although the color scale can vary depending on the ultrasound vendor [34, 35]. A pseudo-quantitative measurement called the strain ratio can be used, which is the ratio of strain measured in adjacent (usually normal) reference tissue region of interest (ROI) to strain measured in a target lesion ROI. A strain ratio > 1 indicates that the target lesion compresses less than the normal reference tissue, indicating lower strain and greater stiffness [36]. In shear-wave elastography (SWE), measurement of the shear-wave speed results in qualitative and quantitative estimates of tissue elasticity [37]. The elasticity measurements, using SWE or 2D SWE, may be expressed as either *shear-wave velocity* (*m/s*) or Young's modulus (kPa) [38].

9.9.1 Endovaginal Elastography

Strain elastography (SE) is a technique of parametric imaging that allows quantification of the elasticity of tissue. Kreutzkamp et al. [39] attempted to determine if the elasticity of paraurethral tissue correlates with urethral mobility and urinary incontinence (UI). One region of interest was placed in the tissue between the urethra and vagina at midlevel of the urethra bordering the urethral wall. The second ROI was set at the level of the os urethra internum in the tissue of the bladder neck in one line to the first ROI. The authors measured elasticity in both ROIs with TDI-Q (Tissue Doppler Imaging-Quantification Software) and calculated the ratio between ROIs. Mobility of the urethra was quantified by measuring the angle between a line parallel to the urethra and a line parallel to the bladder neck during stress and rest. SE analysis was feasible in all cases. A correlation between urethral mobility and elasticity of the paraurethral tissue was found. In case of increasing urethral mobility, the paraurethral tissue close to the bladder neck seems to be more elastic, and the patients reported about more symptoms of UI. No noticeable correlation between UI and urethral elasticity was shown. SE may be a useful technique for direct quantification of tissue elasticity and assessment of pelvic floor biomechanics [39].

Female striated urogenital sphincter contraction measured by shear-wave elastography during pelvic floor muscle activation was described by Aljuraifani et al. [40]. The authors used ultrasound shear-wave elastography (SWE), a noninvasive real-time technique to estimate tissue stiffness. As muscle stiffness can be used as an estimate of muscle force, SWE provides an opportunity to study contraction of the periurethral musculature. Stiffness in a region expected to contain the striated urogenital sphincter (SUS) was quantified using SWE at rest and during a pelvic floor muscle contractions performed at 10%, 25%, and 50% of maximal voluntary contraction (MVC). Two repetitions were performed for 10 s. The authors showed that during contraction, stiffness increased in the region of the SUS in all participants and at all contraction intensities. Multiple regions of increased stiffness were detected, with 95.8% of regions situated ventral to the mid-urethra within the anatomical area of the SUS. The increase in stiffness was greater for 50% MVC than both 10% and 25% MVC contraction intensities ($P < 0.01$). The study has proven that stiffness increases within the anatomical region of the SUS during voluntary pelvic floor muscle contractions with predictable response to changes in contraction intensity. These observations support the potential for ultrasound SWE to study SUS function non-invasively [40] (Fig. 9.17).

Chen et al. [41] described quasistatic elastography with a reference standoff pad as a promising quantitative method evaluating the elastic modulus of the perineal body. The authors used an UltraSONIXR P500 ultrasound system equipped with elastography software. Approximately 1 Hz freehand sinusoidal compression loading of the perineum was used to measure the relative stiffness of the perineal body compared to that of a custom reference standoff pad with a modulus of 36.7 kPa. Measurements were made in 20 healthy nulliparous women. Preliminary data, despite their limitations, provided a first order in vivo estimation of the nulliparous perineal body modulus [41].

Xie et al. [42, 43] evaluated the levator ani before and after Kegel exercise in women with pelvic organ prolapse (POP) stage I/II by transperineal elastography. The patients underwent conventional transperineal ultrasound and elastography. For each patient, the levator ani was located and evaluated in the state of Valsalva. After Kegel exercises for 12 weeks, transperineal ultrasound and elastography were repeated. The elasticity images were assessed using a four-point scale scoring system. The authors showed that the mean elastography score was statistically significantly higher for the levator ani after Kegel exercises (2.90 ± 0.48) than for the baseline score (1.90 ± 0.29) (*p* = 0.025). Transperineal elastography was an effective and useful tool in the evaluation of the levator ani in patients with POP-Q stage I/II before and after Kegel exercises [42, 43].

Masslo et al. [44] introduced elastography as a new method for sonographic assessment of levator avulsion injury in postpartum pelvic floor trauma. The authors showed that the elastographic evaluation revealed more trauma-suspicious lesions than the B-mode investigation. In conclusion sonographic elastography assessment in a new examination plane shows postpartum trauma of the pelvic floor in women after vaginal delivery. This new method may help to identify women with a higher risk of postpartum pelvic floor disorders [44].

Egorov et al. [45, 46] designed a prototype of vaginal tactile imager (VTI) for visualization and assessment of elastic properties of pelvic floor tissues. The prototype of the VTI included a transvaginal probe, an electronic unit, and a laptop computer with a data acquisition card. The vaginal probe
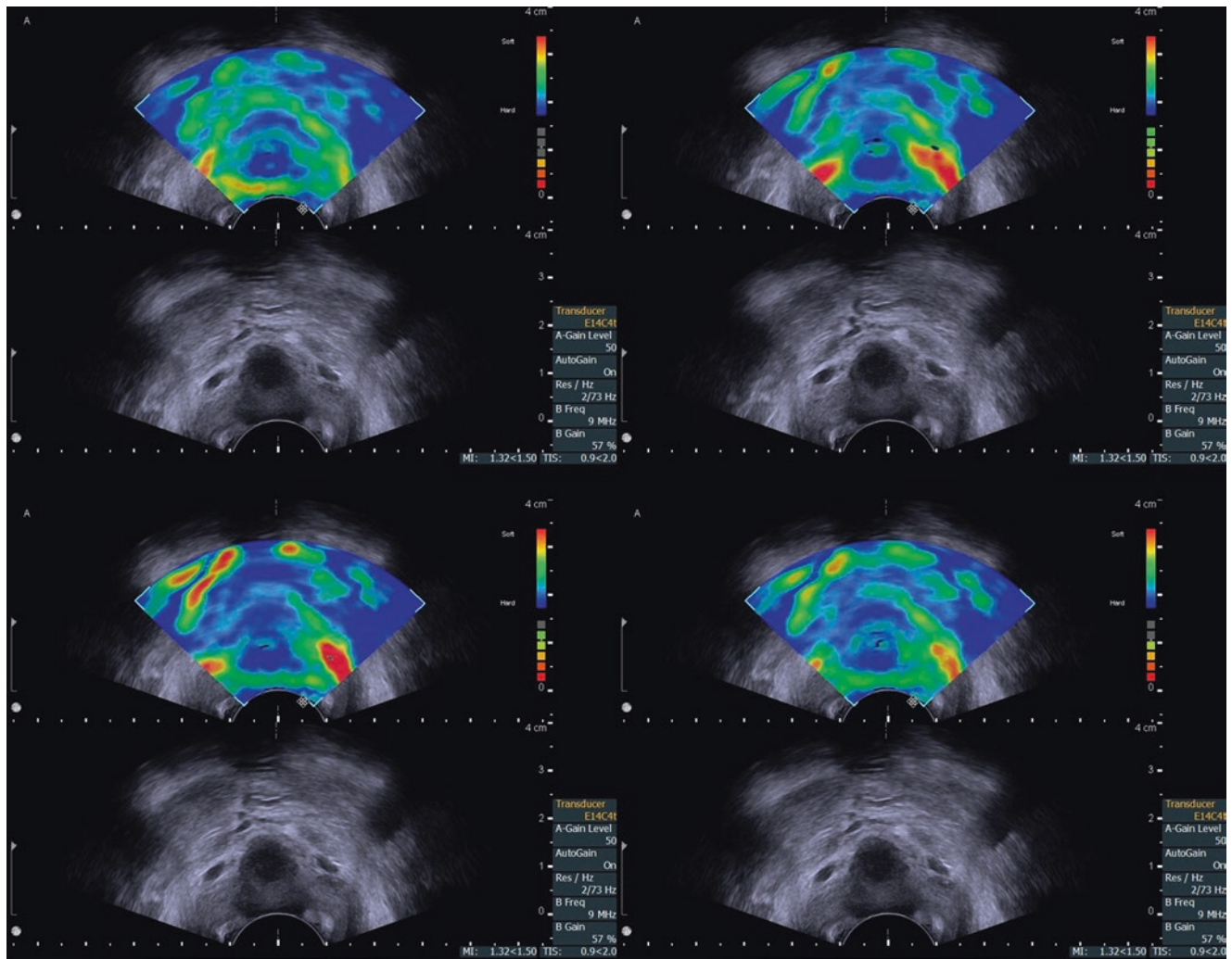
Fig. 9.17 Assessment of urethral complex elasticity in an incontinent female during rest and Valsalva maneuver. Four selected frames demonstrating different elasticity of the urethra and paraurethral structures at various states of urethral contraction/rest. Blue represents low elasticity/high stiffness (hard tissues); red represents high elasticity/low stiffness (soft tissues). Images obtained by the endovaginal ultrasound with E14C4t transducer (BK Medical)

comprised of a tactile sensor array and a tilt sensor. The tactile sensor array is installed on the probe head surface contacting with the vaginal wall during the examination procedure. The probe head measures 48 mm in length, 20 mm in width, and 14 mm in height having ellipsoidal cross section. The tactile sensor array (Pressure Profile Systems, Inc., CA) comprises of 120 capacitive pressure sensors, which provide 2D pressure pattern being contacted with vaginal wall. A pilot clinical study performed with 13 patients demonstrated that tactile imaging allows quantitative evaluation of elastic properties of vaginal walls by means of the elasticity index and has a potential for differentiation of normal tissue and diseased tissue under prolapse condition. VTI allows imaging of a vaginal wall with increased rigidity due to implanted mesh grafts following reconstructive pelvic surgery [45, 46].

Sturm et al. demonstrated that [47] ultrasound shear-wave elastography bladder measurements correlate well with bladder storage pressure and shear-wave speed measurements differ between compliant and noncompliant bladders. This is the first known study to demonstrate that shear-wave elastography is promising as a bedside modality for the assessment of bladder dysfunction in children [47].

9.9.2 Endoanal Elastography

Allgayer et al. [48, 49] analyzed endosonographic elastography of the anal sphincter in patients with fecal incontinence and found that the IAS, a smooth muscle, and the EAS, a striated muscle, have different elastogram color distributions, probably reflecting their different elastic properties.

The absence of significant correlations with the major clinical and functional parameters suggests that in routine clinical practice ultrasound, real-time elastography may not yield additional information in patients with fecal incontinence. There may be exceptions, particularly in irradiated patients [48, 49]. Moreover real-time elastography in patients with fecal incontinence following anorectal surgery with quantitation of sphincter elastic properties yields no further diagnostic and prognostic information compared to conventional EUS in irradiated and non-irradiated patients and, therefore, cannot be regarded as a new tool in the assessment of those patients. Our data further confirm the view that defined sphincter defects may be a major risk factor for an unfavorable outcome [49].

Elastography can distinguish malignant from benign tumors (malignant tumor mean strain ratio value over 1.25 and benign tumor mean strain ratio value below 1.25). In terms of cancer staging, elastography, along with TRUS, is useful to distinguish pT0 stage from pT1 stage, with better results than MRI, including pretreatment biopsy. Elastography, additional to TRUS, does not bring additional information regarding T2 and T3 staging, as TRUS is sufficient for final cancer staging. To our knowledge, the characterization of pathological lymph nodes did not include their elasticity, but, by our experience, these appear more rigid than perirectal fat during elastography [50]. Li et al. demonstrated that SWE is a promising tool that yields valuable quantitative data additional to that provided by ERUS examination in rectal lesions. The cutoff value 61.3 kPa for Emean may serve as a complementary tool in diagnosis of rectal lesions [51].

9.10 Contrast-Enhanced Ultrasound (CEUS)

9.10.1 Rectal Cancer

This application of EAUS has not yet been fully explored in relation to rectal tumors, but there are many studies in other areas of interest, where it has demonstrated its importance in the characterization of tumoral lesions [50]. Immediately after the injection of the contrast medium, the microbubbles reach the rectum, especially the areas where microcirculation is more abundant. The images must be stored for further analysis of loading and unloading curves and for a more objective interpretation, according to the time intervals acquired on these curves. In order to calculate these curves and easily identify the differences between them, one or more ROIs must be manually selected on the equipment, one for the tumor-bearing region and another for an apparently tumor-free region. The most important time-intensity parameters that can be acquired on the loading and unloading curves are the following: contrast arrival time in the ROI (AT), maximum contrast medium enhancement (time to peak, TTP), maximum contrast intensity (peak intensity, PI), area under the curve (AUC), loading time (WIT), ascending slope (AS), and echo intensity (EI) . With the help of these parameters, CEUS offers very good interobserver variability [50, 52, 53].

The contrast agent is homogeneously retained by all rectal adenomas, and, compared to tumor-free rectal wall, the contrast medium becomes visible later and with lower intensity. Difficulty may arise in case of larger adenomas with increased uptake. Adenocarcinomas are irregular, and, compared to the tumor-free rectal wall, the contrast medium loads faster, and contrast maximum enhancement occurs earlier [54]. Specifically, aggressive tumors with high degree of angiogenesis have an increased inhomogeneous contrast uptake. An exception to this rule is that of large tumors with intratumoral necrosis, which can have a low contrast uptake or even no uptake [50]. Enhanced intensity negatively correlates with histologic grade; however, none of other parameters correlates with TNM stage and histologic grade [53].

9.10.2 Contrast-Enhanced Voiding Urosonography (ceVUS)

The most common pediatric application of US contrast agents is contrast-enhanced voiding urosonography (ceVUS), i.e., the intravesical application of US contrast agents via a bladder catheter for the evaluation of vesicoureteral reflux. The procedure and its diagnostic accuracy are well-established and documented [55]. Contrast-enhanced voiding urosonography (ceVUS) has become a well-established method for the diagnosis and treatment monitoring of vesicoureteral reflux (VUR) in children, particularly after the recent approval for this application in children in the USA and in Europe [56]. It is a very safe technique [57, 58], which can be used both in diagnostics and monitoring of treatment of VUR as well as intraoperatively during endoscopic anti-reflux therapy [59]. It enables very accurate assessment of urethra, both in females and in males [60]. Other indications for ceVUS include bladder rupture and urogenital malformation [55].

The introduction of three-dimensional static (3D) and real-time (4D) techniques with ultrasound contrast agents opens up new diagnostic opportunities for this imaging modality [61–63]. 2D ceVUS and 3D/4D ceVUS allow to diagnose the same number of vesicoureteral refluxes; however, there is a statistically significant difference in grading between the two methods. Thus 3D/4D ceVUS appears at least a valid, if not even a more conspicuous technique compared to 2D ceVUS [61–63] (Fig. 9.18).

Contrast-enhanced urosonography (ceVUS) and its modifications such as contrast-enhanced urethrography can be

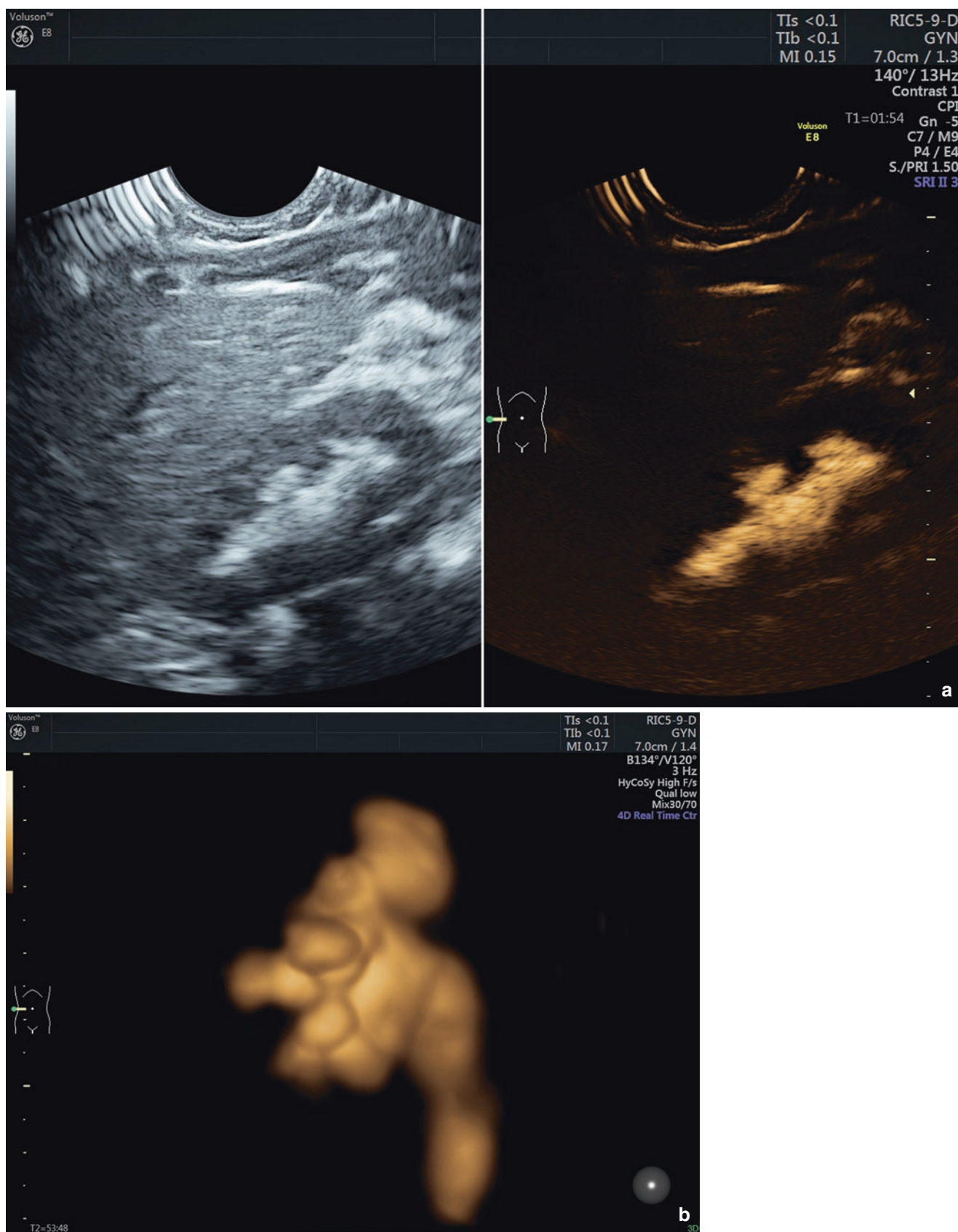**Fig. 9.18** Contrast-enhanced urosonography (ceVUS) in a pediatric patient with recurrent urinary tract infections. Two-dimensional (2D) (**a**) and four-dimensional (4D) (**b**) images of vesicoureteral reflux, according to 2D ceVUS graded as III and according to 4D ceVUS graded as IV. Images obtained by the endovaginal volumetric transducer RIC5-9D (General Electric) from transabdominal access

Fig. 9.19 Contrast-enhanced urethrography in an adolescent female patient with urinary incontinence showing ectopic ureter entering the proximal urethra (arrows). Images obtained by the pediatric volumetric transducer RNA5-9D (General Electric) from transperineal access. *B* bladder, *U* urethra
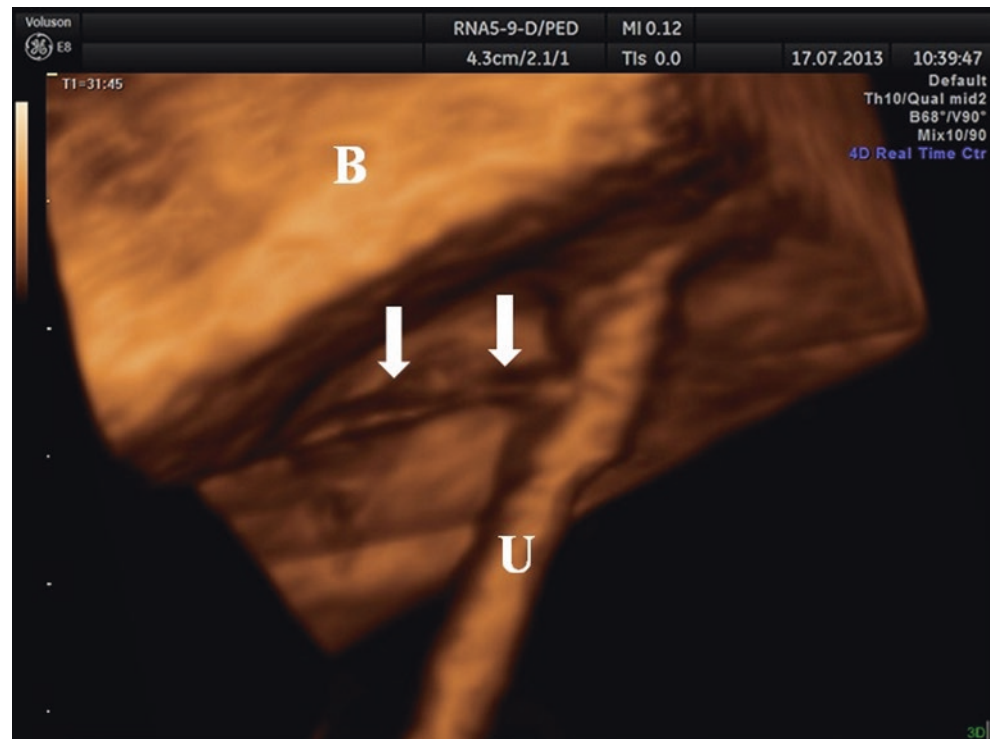
performed also in order to diagnose other congenital abnormalities, e.g., dystopic ureters (Fig. 9.19) or posterior urethral valves in boys [62].

9.10.3 Contrast-Enhanced Ultrasound Genitography

Anorectal malformation is a group of congenital anomalies involving the distal anus and rectum (see chapter Congenital Abnormalities of the Pelvic Floor: Assessment and Management). The diagnosis as such is usually straightforward by clinical inspection and digital palpation. The role of imaging is to give an anatomical overview of the malformation and to assist treatment decisions by providing relevant data on the necessity of immediate surgical intervention, to accurately characterize the complex anatomy of anorectal, cloacal and genitourinary, pelvic, and perineal structures in order to allow for detailed surgical planning and to allow early detection of associated anomalies which is essential to prevent potential life-threatening complications. Contrast-enhanced dynamic US genitography with perineal access is one of the modalities which should be considered in such cases [64].

9.11 Automatic Ultrasound Calculation Systems

Ultrasound technology is rapidly evolving. The development of three-dimensional (3D) ultrasound in late 1980s enabled acquisition and analysis of volume data. This has important implications for clinical practice because assessment of 3D structures with a two-dimensional (2D) imaging modality requires either making assumptions about the shape of the structure or simply ignoring its 3D conformation. A recent development in ultrasound technology is automatic identification and measurement of certain structures within an acquired 3D dataset. These applications aim to facilitate and increase accuracy and reproducibility of ultrasound examinations [65]. Various vendors offer different software, enabling different measurements and post-processing calculations. These include among others software-enabling volume manipulation, analysis and optimization of ultrasound data sets, as well as automatic/semiautomatic calculations, for example, by General Electric (GE), SonoAVC, or by Samsung, 5D.

One of the automatic calculation systems is SonoAVC (automatic volume calculation; GE Medical Systems) or 5D Follicle (Samsung) which is a new software program

designed to provide automatic volume calculations of fluid-filled areas. It is either incorporated into the ultrasound machine or installed on a personal computer for off-line analysis of the datasets acquired by any ultrasound machine of the same manufacturer. SonoAVC/5D Follicle identifies and quantifies hypoechogenic regions within a 3D dataset and provides automatic estimation of their absolute dimensions, mean diameter, and volume. Because each different volume is color-coded separately, the software is an ideal tool for studying follicular development within the ovary. The software is valid and provides accurate measurements [66] and reliable report (Fig. 9.20).

Another type of automatic calculations has been developed for the grading of cystocele.

The transperineal ultrasound (US) has recently emerged as an alternative tool for cystocele grading. The cystocele severity is usually evaluated with the manual measurement of the maximal descent of the bladder (MDB) relative to the symphysis pubis (SP) during Valsalva maneuver. However, this process is time-consuming and operator-dependent. In this study, we propose an automatic scheme for cystocele grading from transperineal US video. A two-layer spatiotemporal regression model is proposed to identify the middle axis and lower tip of the SP and segment the bladder, which are essential tasks for the measurement of the MDB. Both appearance and context features are extracted in the spatiotemporal domain to help the anatomy detection. Experimental results on 85 transperineal US videos show that our method significantly outperforms the state-of-the-art regression method [67].

9.12 Conclusions

A number of new ultrasonographic techniques have been developed recently which carry the potential of significant improvement of the diagnostic value of ultrasound in pelvic floor disorders. Three-dimensional (3D) and real-time four-dimensional (4D) imaging techniques enable to overcome limitations of conventional two-dimensional (2D) US. Complex information on the exact location, extent, and relations of relevant pelvic structures can be displayed with
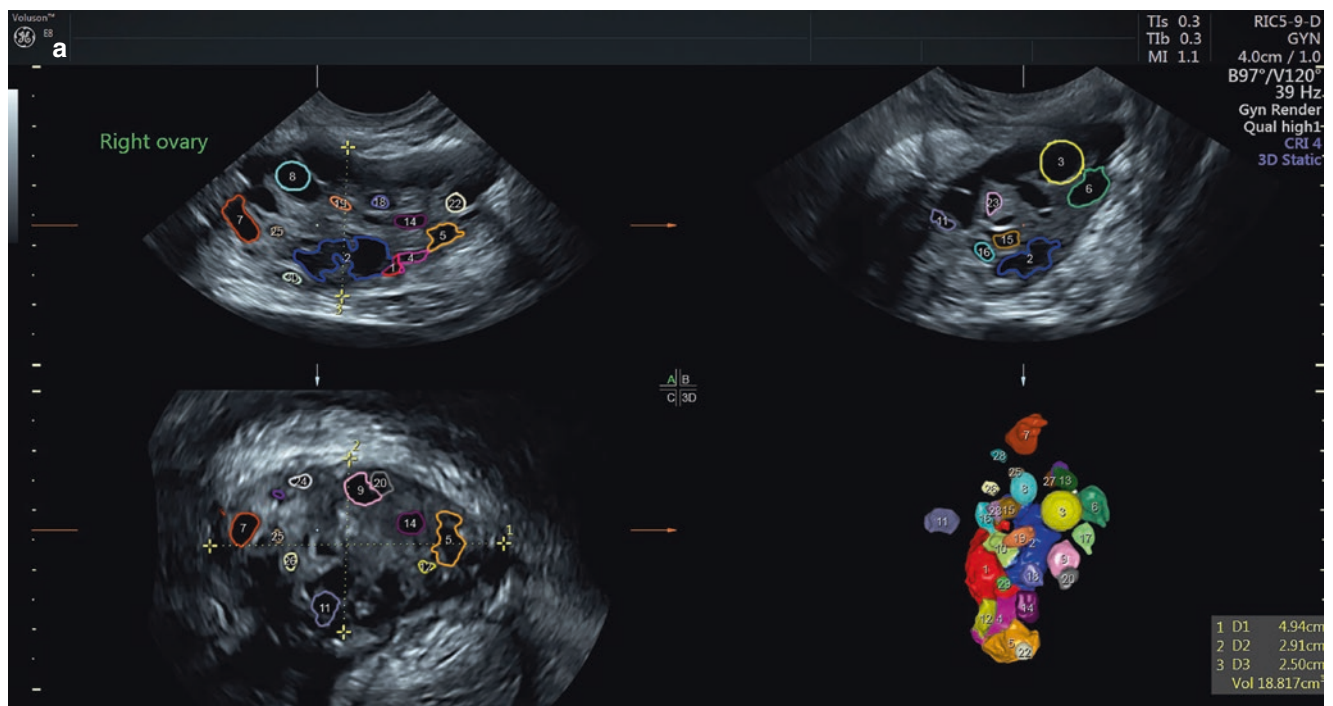
Fig. 9.20 Three-dimensional (3D) endoanal examination of adolescent girl with polycystic ovaries syndrome (PCOS) with the use of SonoAVC—a software enabling automatic calculation of the number, dimensions, and volumes of the ovarian follicles. (**a**) Each follicle is coded automatically with a different color. (**b**) Report from the examination listing each follicle in both ovaries. Images obtained by the endovaginal volumetric transducer RIC5-9D (General Electric) from endoanal access

Gynecology Report

Gynecology Report   Page 1/2

Patient / Exam Information			Date of Exam: •••••

Patient ID	•••••	LMP		Gravida
Name	••••• ••••• •••••	Expected Ovul.		Para
DOB,Age	•••••,16	Day of Cycle		AB
Sex	**Other**	Day of stim.		Ectopic

Perf. Phys.	•••••	Ref. Phys.	•••••	Sonographer	•••••
Comment		Indication			

SonoAVC™ (Semi-)Automatic

Left Ovary

Total#:   24

Right Ovary

Total#:   30

Nr.	d(V) mm	dx mm	dy mm	dz mm	mean d mm	V cm³	Nr.	d(V) mm	dx mm	dy mm	dz mm	mean d mm	V cm³
1	9.6	21.0	8.2	6.1	11.8	0.47	1	9.9	15.9	9.9	7.3	11.0	0.51
2	8.7	13.5	8.7	6.6	9.6	0.34	2	9.7	17.3	9.8	7.2	11.5	0.48
3	7.3	13.4	8.0	4.4	8.6	0.20	3*	7.1	7.3	7.0	7.0	7.1	0.19
4	5.5	7.7	5.7	4.8	6.1	0.09	4	7.0	12.4	6.9	4.4	7.9	0.18
5	5.5	7.5	5.4	4.7	5.9	0.09	5	6.7	10.8	6.3	5.8	7.6	0.15
6	5.4	8.1	5.4	4.8	6.1	0.08	6	5.9	8.3	6.3	4.4	6.4	0.11
7	5.4	7.6	5.7	3.7	5.7	0.08	7	5.8	9.7	5.6	4.8	6.7	0.10
8	5.3	7.4	5.8	3.6	5.6	0.08	8*	5.0	5.6	4.7	4.7	5.0	0.06
9	5.1	6.3	5.9	3.9	5.3	0.07	9	4.9	6.6	5.2	4.1	5.3	0.06
10	5.1	7.8	5.3	3.8	5.6	0.07	10	4.8	6.5	5.4	3.9	5.3	0.06
11	4.8	7.6	5.1	3.0	5.2	0.06	11	4.8	7.2	4.3	3.8	5.1	0.06
12	4.1	5.3	4.5	3.1	4.3	0.04	12	4.2	7.0	3.7	3.1	4.6	0.04
13	4.1	6.5	5.2	2.3	4.7	0.04	13	4.1	5.4	4.3	3.4	4.4	0.04
14	3.7	6.8	4.1	2.2	4.3	0.03	14	4.0	6.2	4.6	2.3	4.4	0.03
15	3.6	5.0	3.9	2.6	3.8	0.03	15	3.9	5.5	3.9	3.1	4.2	0.03
16	3.6	6.3	3.6	2.4	4.1	0.02	16	3.7	5.4	3.7	2.8	4.0	0.03
17	3.6	6.6	3.6	2.1	4.1	0.02	17	3.4	5.2	4.1	2.0	3.8	0.02
18	3.4	4.7	4.0	2.2	3.6	0.02	18	3.4	4.7	4.2	2.1	3.7	0.02
19	2.7	5.0	2.6	2.0	3.2	<0.01	19	3.4	7.3	3.2	1.8	4.1	0.02
20	2.7	4.2	2.7	1.9	2.9	<0.01	20	3.2	4.4	3.6	2.4	3.5	0.02
21	2.5	3.7	2.9	1.6	2.7	<0.01	21	3.2	4.1	3.5	2.3	3.3	0.02
22	2.4	3.8	3.1	1.3	2.7	<0.01	22*	3.1	3.2	3.1	3.1	3.1	0.02
23	2.3	3.3	2.4	1.7	2.5	<0.01	23	3.0	3.9	3.5	2.6	3.3	<0.01
24	2.2	3.6	2.0	1.5	2.4	<0.01	24	3.0	4.0	3.5	2.0	3.2	<0.01
							25	2.8	3.0	2.8	2.6	2.8	<0.01
							26	2.6	4.1	3.0	1.6	2.9	<0.01
							27	2.3	3.4	2.7	1.5	2.5	<0.01
							28	2.3	3.3	2.4	1.6	2.5	<0.01
							29	2.2	2.9	2.7	1.4	2.3	<0.01
							30	2.2	3.9	2.1	1.3	2.5	<0.01

1/2
21.12.2016 10:30:55

Fig. 9.20 (continued)

Name:	•••••		Patient ID:		•••••			

2D Generic	Value	m1	m2	m3	m4	m5	m6	Meth.
Dist.								
D	2.84 cm	0.84	7.44	3.47	1.03	4.04	0.21	avg.
Vol. 3 Dist.								
D1	5.01 cm	4.94	5.08					avg.
D2	2.82 cm	2.91	2.73					avg.
D3	2.28 cm	2.50	2.05					avg.
Vol	16.829 cm³	18.817	14.886					

Date: •••••   Perf. Physician: •••••   Sonographer: •••••

Fig. 9.20 (continued)

the use of 3D techniques. A variety of other advanced ultrasonographic techniques will be increasingly used in the future to provide more detailed information on the morphology and function of examined organs, to facilitate planning and monitoring of surgical procedures, diagnosing postoperative complications, and for surgical training.

Take-Home Messages
- There is a number of recent ultrasound technical innovations including three-dimensional volume render mode, maximum intensity projection, manual segmentation and sculpting, fusion imaging, PixelFlux, framing, color vector mapping, motion tracking, elastography, contrast-enhanced ultrasound, and automatic calculation systems which should be considered in diagnostics of pelvic floor disorders.
- Ultrasound technical innovations carry the potential of much more advanced diagnostics in future clinical practice however require high-end equipment and software and highly professional and well-trained medical personnel.

References

1. Santoro GA, Fortling B. The advantages of volume rendering in three-dimensional endosonography of the anorectum. Dis Colon Rectum. 2007;50:359–68.
2. Dietz HP, Steensma AB. Posterior compartment prolapse on two-dimensional and three-dimensional pelvic floor ultrasound: the distinction between true rectocele, perineal hypermobility and enterocele. Ultrasound Obstet Gynecol. 2005;26:73–7.
3. Mitterberger M, Pinggera GM, Mueller T, Frauscher F, Pallwein L, Gradl J, Peschel R, Bartsch G, Strasser H. Dynamic transurethral sonography and 3-dimensional reconstruction of the rhabdosphincter and urethra: initial experience in continent and incontinent women. J Ultrasound Med. 2006;25:315–20.
4. Santoro GA, Wieczorek AP, Stankiewicz A, Wozniak MM, Bogusiewicz M, Rechberger T. High-resolution three-dimensional endovaginal ultrasonography in the assessment of pelvic floor anatomy: a preliminary study. Int Urogynecol J Pelvic Floor Dysfunct. 2009;20:1213–22.
5. Saba L, Pascalis L, Mallarini G. Multi-detector-row CT of muscles with volume rendering technique. Panminerva Med. 2009;51:43–9.
6. Kuo J, Bredthauer GR, Castellucci JB, von Ramm OT. Interactive volume rendering of real-time three-dimensional ultrasound images. IEEE Trans Ultrason Ferroelectr Freq Control. 2007;54:313–8.
7. Santoro GA, Gizzi G, Pellegrini L, Battistella G, Di Falco G. The value of high-resolution three-dimensional endorectal ultrasonography in the management of submucosal invasive rectal tumors. Dis Colon Rectum. 2009;52:1837–43.
8. Wen L, Li Y, Qing Z, Liu M. Detection of concealed uterine prolapse in the volume-rendering mode of 4-dimensional translabial ultrasound: a retrospective observational study. J Ultrasound Med. 2019;38(7):1705–11.
9. Ohishi H, Hirai T, Yamada R, Hirohashi S, Uchida H, Hashimoto H, Jibiki T, Takeuchi Y. Three-dimensional power Doppler sonography of tumor vascularity. J Ultrasound Med. 1998;17:619–22.
10. Hamazaki N, Kounoike Y, Makinodan K, Nakatani M, Usuba K, Ueda K, Okada T, Egawa S, Takeshita S, Ohishi H, Narita N. Usefulness of three-dimensional color Doppler sonography for the differential diagnosis of subpleural lesions. Nihon Kokyuki Gakkai Zasshi. 2001;39:453–60.
11. Motohide S, Go W, Masahiro O, Hiroshi H, Masaki K. Clinical application of three-dimensional ultrasound imaging as intraoperative navigation for liver surgery. Nihon Geka Gakkai zasshi. 1998;99:203–7.
12. Wieczorek AP, Wozniak MM, Stankiewicz A. Quantification of urethral vascularity with high-frequency endovaginal ultrasonography. Preliminary report in nulliparous females. 2009 (personal communication).
13. Rothenberg F, Fisher SA, Watanabe M. Sculpting the cardiac outflow tract. Birth Defects Res C Embryo Today. 2003;69:38–45.
14. Kim SK, Choi HJ, Park SY, Lee HY, Seo SS, Yoo CW, Jung DC, Kang S, Cho KS. Additional value of MR/PET fusion compared with PET/CT in the detection of lymph node metastases in cervical cancer patients. Eur J Cancer. 2009;45:2103–9.
15. Singh AK, Kruecker J, Xu S, Glossop N, Guion P, Ullman K, Choyke PL, Wood BJ. Initial clinical experience with real-time transrectal ultrasonography-magnetic resonance imaging fusion-guided prostate biopsy. BJU Int. 2008;101:841–5.
16. Selli C, Caramella D, Giusti S, Conti A, Tognetti A, Mogorovich A, De Maria M, Bartolozzi C. Value of image fusion in the staging of prostatic carcinoma. Radiol Med. 2007;112:74–81.
17. Ignee A, Dong Y, Schuessler G, Baum U, Dietrich CF. Endorectal fusion imaging: a description of a new technique. Endosc Ultrasound. 2017;6:241–4.
18. Mukherji SK, Rosenman JG, Soltys M, Boxwala A, Castillo M, Carrasco V, Pizer SM. A new technique for CT/MR fusion for skull base imaging. Skull Base Surg. 1996;6:141–6.
19. Scholbach T, Herrero I, Scholbach J. Dynamic color Doppler sonography of intestinal wall in patients with Crohn disease compared with healthy subjects. J Pediatr Gastroenterol Nutr. 2004;39:524–8.
20. Scholbach T, Girelli E, Scholbach J. Dynamic tissue perfusion measurement: a novel tool in follow-up of renal transplants. Transplantation. 2005;79:1711–6.
21. Wieczorek AP, Wozniak MM, Stankiewicz A. The assessment of normal female urethral vascularity with Color Doppler endovaginal ultrasonography: preliminary report. Pelviperineology. 2009;28:59–61.
22. Lone F, Sultan AH, Stankiewicz A, Thakar R, Wieczorek AP. Vascularity of the urethra in continent women using colour Doppler high-frequency endovaginal ultrasonography. Springerplus. 2014;3:619.
23. Lone F, Thakar R, Wieczorek AP, Sultan AH, Stankiewicz A. Assessment of urethral vascularity using 2D colour Doppler high-frequency endovaginal ultrasonography in women treated for symptomatic stress urinary incontinence: 1-year prospective follow-up study. Int Urogynecol J. 2016;27:85–92.
24. Yeniel AO, Ergenoglu AM, Meseri R, Kismali E, Ari A, Kavukcu G, Aydin HH, Ak H, Atay S, Itil IM. Is overactive bladder microvasculature disease a component of systemic atherosclerosis? Neurourol Urodyn. 2018;37:1372–9.
25. Pregazzi R, Sartore A, Bortoli P, Grimaldi E, Troiano L, Guaschino S. Perineal ultrasound evaluation of urethral angle and bladder neck mobility in women with stress urinary incontinence. BJOG. 2002;109:821–7.

26. Rahmanian S, Jones R, Peng Q, Constantinou CE. Visualization of biomechanical properties of female pelvic floor function using video motion tracking of ultrasound imaging. Stud Health Technol Inform. 2008;132:390–5.

27. Huang YL, Chen HY. Computer-aided diagnosis of urodynamic stress incontinence with vector-based perineal ultrasound using neural networks. Ultrasound Obstet Gynecol. 2007;30:1002–6.

28. Reddy AP, DeLancey JO, Zwica LM, Ashton-Miller JA. On-screen vector-based ultrasound assessment of vesical neck movement. Am J Obstet Gynecol. 2001;185:65–70.

29. Peng Q, Jones R, Shishido K, Constantinou CE. Ultrasound evaluation of dynamic responses of female pelvic floor muscles. Ultrasound Med Biol. 2007;33:342–52.

30. Constantinou CE (2009) Dynamics of female pelvic floor function using urodynamics, ultrasound and Magnetic Resonance Imaging (MRI). Eur J Obstet Gynecol Reprod Biol. 144 Suppl 1: S159–165.

31. Chlebiej M, Nowiński K, Ścisło P, Bała P. Reconstruction of heart motion from 4D echocardiographic images. In: Kropatsch WG, Kampel M, Hanbury A, editors. Computer analysis of images and patterns. Lecture notes in computer science, vol. 4673. Berlin: Springer-Verlag; 2007. p. 245–52.

32. Chlebiej M, Nowiński K, Ścisło P, Bała P. Heart motion visualization tools for 4D echocardiographic images. J Med Informat Technol. 2007;11:177–84.

33. Bamber J, Cosgrove D, Dietrich CF, Fromageau J, Bojunga J, Calliada F, Cantisani V, Correas JM, D'Onofrio M, Drakonaki EE, Fink M, Friedrich-Rust M, Gilja OH, Havre RF, Jenssen C, Klauser AS, Ohlinger R, Saftoiu A, Schaefer F, Sporea I, Piscaglia F. EFSUMB guidelines and recommendations on the clinical use of ultrasound elastography. Part 1: basic principles and technology. Ultraschall Med. 2013;34:169–84.

34. Gennisson JL, Deffieux T, Fink M, Tanter M. Ultrasound elastography: principles and techniques. Diagn Interv Imaging. 2013;94:487–95.

35. Bhatia KS, Lee YY, Yuen EH, Ahuja AT. Ultrasound elastography in the head and neck. Part I. Basic principles and practical aspects. Cancer Imaging. 2013;13:253–9.

36. Choi YJ, Lee JH, Baek JH. Ultrasound elastography for evaluation of cervical lymph nodes. Ultrasonography. 2015;34:157–64.

37. Sigrist RMS, Liau J, Kaffas AE, Chammas MC, Willmann JK. Ultrasound elastography: review of techniques and clinical applications. Theranostics. 2017;7:1303–29.

38. Mulabecirovic A, Mjelle AB, Gilja OH, Vesterhus M, Havre RF. Repeatability of shear wave elastography in liver fibrosis phantoms—evaluation of five different systems. PLoS One. 2018;13:e0189671.

39. Kreutzkamp JM, Schafer SD, Amler S, Strube F, Kiesel L, Schmitz R. Strain elastography as a new method for assessing pelvic floor biomechanics. Ultrasound Med Biol. 2017;43:868–72.

40. Aljuraifani R, Stafford RE, Hug F, Hodges PW. Female striated urogenital sphincter contraction measured by shear wave elastography during pelvic floor muscle activation: proof of concept and validation. Neurourol Urodyn. 2018;37:206–12.

41. Chen L, Low LK, DeLancey JO, Ashton-Miller JA. In vivo estimation of perineal body properties using ultrasound quasistatic elastography in nulliparous women. J Biomech. 2015;48:1575–9.

42. Xie M, Zhang X, Zhang X, Wang W, Hua K. Can we evaluate the levator ani after Kegel exercise in women with pelvic organ prolapse by transperineal elastography? A preliminary study. J Med Ultrason. 2018;45:437–41.

43. Xie M, Zhang X, Liu J, Ding J, Ren Y, Hua K. Evaluation of levator ani with no defect on elastography in women with POP. Int J Clin Exp Med. 2015;8:10204–12.

44. Masslo K, Mollers M, de Murcia KO, Klockenbusch W, Schmitz R. New method for assessment of levator avulsion injury: a comparative elastography study. J Ultrasound Med. 2018;

45. Egorov V, van Raalte H, Sarvazyan AP. Vaginal tactile imaging. IEEE Trans Biomed Eng. 2010;57:1736–44.

46. van Raalte H, Egorov V. Tactile imaging markers to characterize female pelvic floor conditions. Open J Obstet Gynecol. 2015;5:505–15.

47. Sturm RM, Yerkes EB, Nicholas JL, Snow-Lisy D, Diaz Saldano D, Gandor PL, Halline CG, Rosoklija I, Rychlik K, Johnson EK, Cheng EY. Ultrasound shear wave elastography: a novel method to evaluate bladder pressure. J Urol. 2017;198:422–9.

48. Allgayer H, Ignee A, Dietrich CF. Endosonographic elastography of the anal sphincter in patients with fecal incontinence. Scand J Gastroenterol. 2010;45:30–8.

49. Allgayer H, Ignee A, Zipse S, Crispin A, Dietrich CF. Endorectal ultrasound and real-time elastography in patients with fecal incontinence following anorectal surgery: a prospective comparison evaluating short- and long-term outcomes in irradiated and non-irradiated patients. Zeitschrift fur Gastroenterologie. 2012;50:1281–6.

50. Badea R, Gersak MM, Dudea SM, Graur F, Hajjar NA, Furcea L. Characterization and staging of rectal tumors: endoscopic ultrasound versus MRI/CT. Pictorial essay. Med Ultrason. 2015;17:241–7.

51. Li T, Lu M, Li Y, Li J, Hu Z, Li X, Cheng X, Jiang J, Tan B. Quantitative elastography of rectal lesions: the value of shear wave elastography in identifying benign and malignant rectal lesions. Ultrasound Med Biol. 2019;45:85–92.

52. Zhuang H, Yang ZG, Wang ZQ, Wang XD, Chen HJ, Zhang YC, Luo Y. Features of time-intensity curve parameters of colorectal adenocarcinomas evaluated by double-contrast enhanced ultrasonography: initial observation. Eur J Radiol. 2012;81:677–82.

53. Wang Y, Li L, Wang YX, Cui NY, Zou SM, Zhou CW, Jiang YX. Time-intensity curve parameters in rectal cancer measured using endorectal ultrasonography with sterile coupling gels filling the rectum: correlations with tumor angiogenesis and clinicopathological features. Biomed Res Int. 2014;2014:587806.

54. Lu M, Yan B, Song J, Ping W, Yue LX, Song B. Double-contrast-enhanced sonography for diagnosis of rectal lesions with pathologic correlation. J Ultrasound Med. 2014;33:575–83.

55. Riccabona M, Vivier P-H, Ntoulia A, Darge K, Avni F, Papadopoulou F, Damasio B, Ording-Muller L-S, Blickman J, Lobo M-L, Willi U. ESPR uroradiology task force imaging recommendations in paediatric uroradiology, part VII: standardised terminology, impact of existing recommendations, and update on contrast-enhanced ultrasound of the paediatric urogenital tract. Pediatr Radiol. 2014;44:1478–84.

56. Riccabona M, Lobo ML, Augdal TA, Avni F, Blickman J, Bruno C, Damasio MB, Darge K, Mentzel H-J, Napolitano M, Ntoulia A, Papadopoulou F, Petit P, Woźniak MM, Ording-Müller L-S. European Society of Paediatric Radiology Abdominal Imaging Task Force recommendations in paediatric uroradiology, part X: how to perform paediatric gastrointestinal ultrasonography, use gadolinium as a contrast agent in children, follow up paediatric testicular microlithiasis, and an update on paediatric contrast-enhanced ultrasound. Pediatr Radiol. 2018;48:1528–36.

57. Riccabona M, Mentzel H-J. Contrast agents in childhood: application and safety considerations. In: Riccabona M, editor. Pediatric urogenital radiology. Cham: Springer International Publishing; 2018. p. 123–31.

58. Papadopoulou F, Ntoulia A, Siomou E, Darge K. Contrast-enhanced voiding urosonography with intravesical administration of a second-generation ultrasound contrast agent for diagnosis of vesicoureteral reflux: prospective evaluation of contrast safety in 1,010 children. Pediatr Radiol. 2014;44:719–28.

59. Wozniak MM, Osemlak P, Pawelec A, Brodzisz A, Nachulewicz P, Wieczorek AP, Zajaczkowska MM. Intraoperative contrast-enhanced urosonography during endoscopic treatment of vesico-ureteral reflux in children. Pediatr Radiol. 2014;44:1093–100.

60. Duran C, del Riego J, Riera L, Martin C, Serrano C, Palana P. Voiding urosonography including urethrosonography: high-quality examinations with an optimised procedure using a second-generation US contrast agent. Pediatr Radiol. 2012;42:660–7.

61. Wozniak MM, Osemlak P, Ntoulia A, Borzecka H, Bienias B, Brodzisz A, Jedrzejewski G, Drelich-Zbroja A, Powerski M, Pech M, Wieczorek AP. 3D/4D contrast-enhanced urosonography (ceVUS) in children—is it superior to the 2D technique? J Ultrasonograph. 2018;18:120–5.

62. Wozniak MM, Pawelec A, Wieczorek AP, Zajaczkowska MM, Borzecka H, Nachulewicz P. 2D/3D/4D contrast-enhanced voiding urosonography in the diagnosis and monitoring of treatment of vesicoureteral reflux in children—can it replace voiding cystoure-thrography? J Ultrasonograph. 2013;13:394–407.

63. Wozniak MM, Wieczorek AP, Pawelec A, Brodzisz A, Zajaczkowska MM, Borzecka H, Nachulewicz P. Two-dimensional (2D), three-dimensional static (3D) and real-time (4D) contrast enhanced voiding urosonography (ceVUS) versus voiding cysto-urethrography (VCUG) in children with vesicoureteral reflux. Eur J Radiol. 2016;85:1238–45.

64. Riccabona M, Lobo M-L, Ording-Muller L-S, Thomas Augdal A, Fred Avni E, Blickman J, Bruno C, Damasio B, Darge K, Ntoulia A, Papadopoulou F, Vivier P-H. European Society of Paediatric Radiology abdominal imaging task force recommendations in paediatric uroradiology, part IX: imaging in anorectal and cloacal malformation, imaging in childhood ovarian torsion, and efforts in standardising paediatric uroradiology terminology. Pediatr Radiol. 2017;47:1369–80.

65. Ata B, Tulandi T. Ultrasound automated volume calculation in reproduction and in pregnancy. Fertil Steril. 2011;95:2163–70.

66. Raine-Fenning N, Jayaprakasan K, Clewes J, Joergner I, Bonaki SD, Chamberlain S, Devlin L, Priddle H, Johnson I. SonoAVC: a novel method of automatic volume calculation. Ultrasound Obstet Gynecol. 2008;31:691–6.

67. Ni D, Ji X, Gao Y, Cheng JZ, Wang H, Qin J, Lei B, Wang T, Wu G, Shen D. Automatic cystocele severity grading in ultrasound by spatio-temporal regression. Med Image Comput Comput Assist Interv. 2016;9901:247–55.